General Disclaimer

One or more of the Following Statements may affect this Document

- This document has been reproduced from the best copy furnished by the organizational source. It is being released in the interest of making available as much information as possible.

- This document may contain data, which exceeds the sheet parameters. It was furnished in this condition by the organizational source and is the best copy available.

- This document may contain tone-on-tone or color graphs, charts and/or pictures, which have been reproduced in black and white.

- This document is paginated as submitted by the original source.

- Portions of this document are not fully legible due to the historical nature of some of the material. However, it is the best reproduction available from the original submission.

ERT

Final Report
Document P-1068F
April 1976
Contract No. NAS 5-20868

Prepared for
Goddard Space Flight Center
Greenbelt, Maryland 20771

The development of a model to infer precipitation from microwave measurements

Mary Grace Fowler
Kenneth R. Hardy
Nien Dak Sze

ENVIRONMENTAL RESEARCH & TECHNOLOGY, INC.
CONCORD, MASS. • CHICAGO • LOS ANGELES • WASHINGTON, D.C.

1. Report No.	2. Government Accession No.	3. Recipient's Catalog No.

4. Title and Subtitle	5. Report Date
The Development of a Model to Infer Precipitation from Microwave Measurements	April 1976
	6. Performing Organization Code
7. Author(s)	8. Performing Organization Report No.
Mary Grace Fowler, Kenneth R. Hardy and Nien Dak Sze	P-1068
	10. Work Unit No.
9. Performing Organization Name and Address	11. Contract or Grant No.
Environmental Research & Technology, Inc. 696 Virginia Road Concord, MA 01742	NAS5-20868
	13. Type of Report and Period Covered
12. Sponsoring Agency Name and Address	
National Aeronautics & Space Administration Washington, D.C. 20546	14. Sponsoring Agency Code

15. Supplementary Notes

Technical Officer: James R. Greaves
Goddard Space Flight Center
Greenbelt, Maryland

16. Abstract

To permit the inference of precipitation amounts from radiometric measurements, a radiative interaction model has been developed. This model uses a simple computational scheme to determine the effects of rain upon brightness temperatures and can be used with a statistical inversion procedure to invert for rain rate. Precipitating cloud models have also been developed and used with the microwave model for frequencies of 19.35 and 37 GHz to determine the variability of the microwave-rain rate relationship on a global and seasonal basis.

17. Key Words (Suggested by Author(s))	18. Distribution Statement
Precipitation Microwave Radiation Radiometric Models Rain Drop Size Distribution	Unclassified - Unlimited

19. Security Classif. (of this report)	20. Security Classif. (of this page)	21. No. of Pages	22. Price*
Unclassified	Unclassified	64	

*For sale by the Clearinghouse for Federal Scientific and Technical Information
Springfield, Virginia 22151

ACKNOWLEDGMENTS

The authors would like to express their appreciation to Dr. Thomas T. Wilheit, Jr. of NASA Goddard Space Flight Center for the cooperation and technical guidance he provided in the development of the radiometric model. They would also like to thank Ms. Nancy Tripp for patiently developing, modifying and running the computer simulation model, and Messrs. David T. Chang and Ronald G. Isaacs for their contributions to this program.

TABLE OF CONTENTS

LIST OF FIGURES

LIST OF FIGURES (cont)

1. INTRODUCTION

The accurate determination of rainfall is of great importance to the Global Atmospheric Research Program (GARP) because it provides a reliable indication of the organization and areal extent of convection, the amount and distribution of latent heat release and the upward mass flux. However, accurate determination of rainfall on a global basis requires the use of advanced techniques such as microwave remote sensing since conventional surface measurements are made only at selected sites and visible and infrared radiometers do not sense rain directly. Use of microwave remote sensing, in turn, requires a thorough understanding of the relationship between rain rate and brightness temperature and a knowledge of the atmospheric conditions which affect this relationship.

To determine the relationship between precipitation and microwave measurements, Environmental Research & Technology, Inc. (ERT) developed a simulation model which employed a noniterative technique to assess the effects of absorption and scattering by raindrops upon microwave radiation. This model, which showed the existence of a unique relationship between rain rate and brightness temperature, has been documented in Gaut, et. al. (1974). However, because of certain assumptions made about the microstructure and macrostructure of rain clouds, it was felt that the derived relationship might not be universally applicable and that further investigation was necessary to permit the global inference of rain rates.

This report presents the results of a study which modified and generalized ERT's precipitation model and which developed and simulated cloud models and atmospheric conditions appropriate to differing seasons and latitudes. As a result of this simulation, it was found that variations in drop size spectra have only a minimal impact on the brightness temperature-rain rate relationship, but that variations in atmospheric structure caused marked changes. Section 2 will discuss the precipitation model in its original and modified form and the assumptions and limitations of this model. Section 3 will present the derived cloud and atmospheric models, and the results of the relationship between rain rate and brightness temperature for each set of conditions or models is given in Section 4. Section 5 summarizes the effects of precipitation on microwave remote sensing and provides recommendations for the operational determination of rainfall on a global basis.

2. THE RADIOMETRIC MODEL OF PRECIPITATION EFFECTS

2.1 Background

Precipitation size droplets are the primary contributors of nonresonant opacity in the microwave region and thus it is natural to suppose that information about precipitation may be inferred directly from microwave measurements. However, such inference requires an evaluation of the effects of scattering and absorption by large droplets on microwave radiation, the exact determination of which necessitates the solution of computationally complex scattering functions and interaction models. The goal of ERT's development of a precipitation model, described below, was to permit an evaluation of precipitation effects through the use of an extinction approximation model which would be computationally efficient.

The model is basically an analytical extension of an existing approximation model for the analysis of clouds. The development recognizes that the essential difference between precipitating and nonprecipitating clouds is in the nature of their respective drop size distributions. The radiative properties of nonprecipitating clouds may be derived by assuming individual cloud droplets to be Rayleigh scatterers and integrating over the range of cloud droplet sizes. This leads to an analytical form for the cloud extinction coefficient whose properties in the centimeter wavelength region have been evaluated (Staelin, 1966; Gaut and Reifenstein, 1970). Unfortunately, precipitation droplets are one to two orders of magnitude larger than cloud droplets, and the Rayleigh approximation breaks down (Westwater, 1972). A general solution to the problem is available in the form of the Mie (1908) theory solutions. However, the extinction efficiency factor must be computed for each drop size and temperature at a given wavelength and then integrated across the distribution of droplet sizes within the ensemble in order to yield the extinction coefficient. This calculation would involve significant expense if implemented within the intricacies of an operational computation scheme. Thus, there is a distinct advantage to employing an approximation.

In the approach used to develop this approximation, the analysis consisted of three basic parts:

1) Examination of the interaction between the radiation field and individual precipitation droplets (for which the index of refraction is known as a function of frequency and temperature).

2) Determination of unit volume (intensive) radiative transfer properties of an assumed drop size distribution.

3) Determination of the geometry dependent (extensive) effects using the equation of radiative transfer.

During an earlier study (Gaut, et. al., 1974) these three problems were studied and discussed in terms of their applicability to a selected precipitating cloud model. In this study, the three phases were reexamined leading to modifications in several aspects of the precipitation model and generalization of its applicability to a wide variety of precipitation conditions. This section will thus discuss the preliminary approximation, the modifications to this approximation, and the assumptions and limitations of the resulting approach.

2.2 Theoretical Development

The unit volume extinction coefficient due to an ensemble of droplets is given by the integral of the extinction cross section for a droplet of given radius times the drop size distribution function:

$$\gamma_E\left(\tilde{n}(\lambda,T),\lambda\right) = \int_0^\infty N(r)\, Q_E\left(\tilde{n}(\lambda,T),\lambda,r\right)\, r^2\, dr \qquad (2\text{-}1)$$

where

γ_E is unit volume extinction coefficient (neper m^{-1}).

$N(r)$ is drop size distribution function ($cm^{-3}\ \mu m^{-1}$).

Q_E is the Mie efficiency factor for extinction.

$\tilde{n}(\lambda,T)$ is the complex index of refraction (dimensionless).

λ is wavelength (cm).

r is drop radius (μm).

T is absolute temperature (°K).

The efficiency factor (which is a function of temperature, droplet radius, and wavelength) is obtained from the solution to the problem of diffraction of a plane monochromatic wave by a homogeneous dielectric sphere of arbitrary radius (Mie, 1908):

$$Q_E = \frac{2}{q^2} \sum_{\ell=1}^{\infty} (2\ell + 1)\ \mathrm{Re}\ \left[a_\ell\ (\tilde{n}(\lambda,T),q) + b_\ell\ (\tilde{n}(\lambda,T),q)\right] \qquad (2\text{-}2)$$

where the coefficients a_ℓ and b_ℓ in the Mie series are obtained by the boundary conditions at the surface of the sphere and at infinity, and where $q = [2\pi r/(\lambda \times 10^4)]$ is called the dimensionless drop size parameter, a measure of the phase shift across the droplet.

The complex index of refraction of water at centimeter wavelengths is given by the Debye Formula (1929):

$$\tilde{n}^2 = \frac{\varepsilon_o - \varepsilon_\infty}{1 + i(\lambda_0/\lambda)} + \varepsilon_\infty \ . \qquad (2\text{-}3)$$

Here ε_o and ε_∞ are the static and optical dielectric constants and λ_o is the Debye relaxation wavelength. The constants are temperature dependent and their values are calculated using the values of Grant, et. al. (1957).

Since the complex index of refraction, $\tilde{n}$, is a function of temperature and wavelength, $Q_E\ (\tilde{n},\lambda,r)$ must be specified for each λ and T, as well as for each r. Due to the series summation in Expression 2-2, this is not an easy matter computationally.

2.3 Rayleigh Limit - Staelin Approximation

An alternative form for the Mie extinction efficiency factor is given by a power series expansion in the dimensionless drop size parameter.

$$Q_E(\lambda,r,T) = qZ(\lambda,T) + q^3 A(\lambda,T) + q^4 B(\lambda,T) + \ldots \qquad (2\text{-}4)$$

where

$$Z = 4\ \mathrm{Im}\{-K\} = 4\ \mathrm{Im}\left(-\frac{\tilde{n}^2 - 1}{\tilde{n}^2 + 2}\right)$$

$$A = -\frac{4}{5}\ \mathrm{Im}\left(\frac{\tilde{n}^2 - 1}{\tilde{n}^2 + 2}\ \frac{\tilde{n}^4 + 27\tilde{n}^2 + 38}{2\tilde{n}^2 + 3}\right)$$

$$B = 8/3\ \mathrm{Re}\ \frac{\tilde{n}^2 - 1}{\tilde{n}^2 + 2}\,.$$

This expansion is valid for all q, but is especially useful in the limit where $q << 1$, i.e., when the wavelength of interest is much larger than the droplet size. At microwave wavelengths this holds true for nonprecipitating clouds.

In this limit, the Mie solution has the following asymptotic behavior:

$q \to 0$; $Q_E \to qZ(\lambda,T)$. Rayleigh Limit (small droplets)

For nonprecipitating clouds the average droplet radii range from 10^0 to 10^2 um. At a wavelength of 1 cm, the q parameter is thus of the order of 10^{-3} to 10^{-2}, i.e., $q << 1$. This falls within the Rayleigh limit region.

Substituting into Expression 2-1,

$$\gamma_E = \int_0^\infty N(r)\ qZ(\lambda,T)\ \pi r^2\ dr = mF(\lambda,T) \qquad (2\text{-}5)$$

where

$m = \frac{4\pi\rho}{3} \int_0^\infty N(r)\ r^3\ dr$ is the mass density of the droplet ensemble

and

$F(\lambda,T)$ is a function of wavelength and temperature only. This function has been evaluated empirically by Staelin (1966) for which the expression becomes:

$$\gamma_E = \frac{1.0016 \times 10^4 \text{ m } 10^{0.0122(291-T)}}{2} \quad \text{(neper m}^{-1}\text{)}. \qquad (2\text{-}6)$$

This says that the unit volume extinction of a nonprecipitating cloud is proportional to its mass density regardless of the nature of the droplet distribution. This is not true, however, for a precipitating cloud and this approach is not applicable.

2.4 The ERT Precipitation Extinction Approximation

The approximation to be used for precipitating clouds is based on the character of the variation of Q_E (λ,r,T) with r and the nature of the relevant drop size distribution function N(r). The upper portion of Figure 2-1 portrays the range of droplet radii for fair weather cumulus, cumulus congestus, and rain with a rainfall rate of 25.4 mm hr^{-1}. The broken line indicates the variation of Q_E (λ,r,T) with r at λ = 1.0 cm and T = 298°K. Note that while the size distributions of nonprecipitating clouds (Cu) are limited to the Rayleigh region, the rainfall distribution extends through the transition region to the large sphere region where the asymptotic limit of the Mie series (Expression 2-2) approaches 2:

$$q \to \infty;\ Q_E \to 2. \qquad \text{Large Sphere Limit}$$

An average raindrop has a characteristic radius on the order of 10^3 μm. At a wavelength of 1 cm, the q parameter is of order 1. The Rayleigh limit is no longer valid and, furthermore, it must be recognized that the extinction factor will vary orders of magnitude within the size range of the rainfall droplets. For complete accuracy, the full Mie Theory using Equation 2-2 should be used in this range of drop sizes. This would be feasible if all raindrops had the same radius and the atmospheric temperature structure was isothermal. However, the

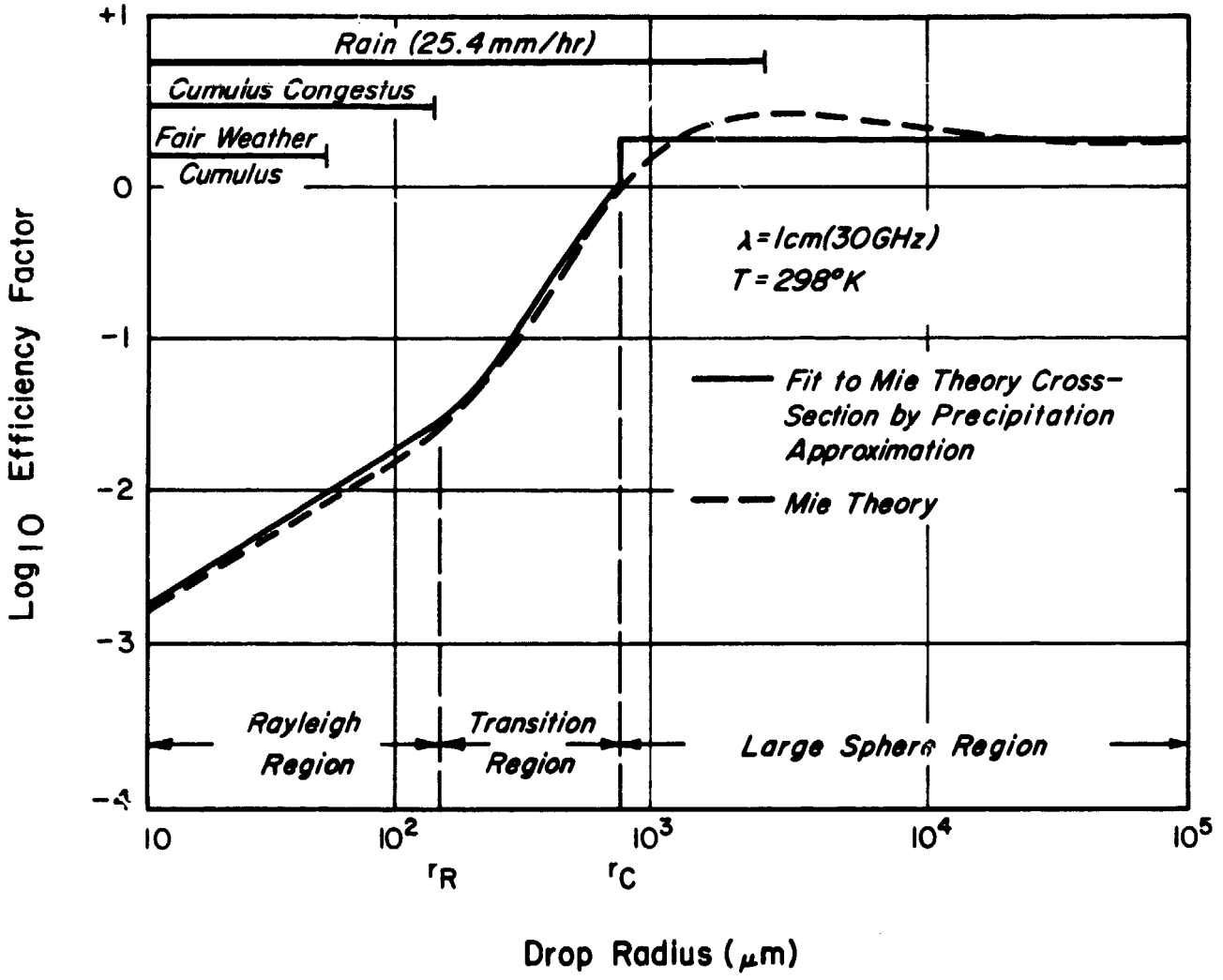

Figure 2-1 Range of Drop Sizes and Mie Efficiency Factors for Full Mie Theory and Linear Segment Approximation.

natural distributions of droplet radius and atmospheric vertical temperature structure make a layered computation using Equation 2-2 computationally complex.

The approach taken here was to assume that the Mie expression (Equation 2-4) could be approximated by a small number of terms and that this number of terms can be assumed to be dependent on the size range of the droplets such that the attenuation coefficient can be expressed as:

$$\gamma_E = \int_0^\infty N(r)\, Q_E\,(r,\lambda,T)\, \pi r^2\, dr$$

$$\simeq \int_0^{r_1} N(r)\, Q_E\,(r)\, \pi r^2\, dr + \int_{r_1}^{r_2} N(r)\, Q_E\,(r)\, \pi r^2\, dr$$

$$+ \ \ldots\ \ldots \int_{r_n}^{\infty} N(r)\, Q_E\,(r)\, \pi r^2\, dr \qquad (2\text{-}7)$$

for n + 1 size intervals.

As a preliminary approximation to γ_ε (Gaut, et. al., 1974), three representative regions were selected:

(a) Region I - Rayleigh limit region $r < r_R$

(b) Region II - Transition region $r_R \leq r \leq r_c$

(c) Region III - Large sphere region $r_c < r$

where the approximations to the Mie efficiency factors in the three regions were as follows:

$$\begin{aligned} Q_E &= qZ && \text{for (Region I) } r < r_R \\ &= qZ + Aq^3 + Bq^4 && \text{for (Region II) } r_R \leq r \leq r_c \\ &= 2 && \text{for (Region III) } r_c < r \end{aligned} \qquad (2\text{-}8)$$

The quantities q, Z, A, and B are as previously defined.

The limits r_c and r_R are specified in the following manner. The upper limit to the Rayleigh region is taken where the dimensionless drop size parameter reaches 0.10. This is approximately the point at which the q^3 term in Equation 2-4 reaches ten percent of the leading term in q. Thus,

$$q_R = 0.10$$

and

$$r_R = (1.59 \times 10^2)\lambda.$$

The lower limit of the large sphere region is located by specifying the position of the optical resonance region. The general criteria adopted is:

$$r_c = \frac{\lambda \times 10^4}{2|\tilde{n}|}$$

where

$$|\tilde{n}| > \pi.$$

The fit of this approximation to the Mie Theory is demonstrated in Figure 2-1 and is quite reasonable.

However, during this current study reexamination of this approximation indicated that it would be improved by the addition of a fourth region. As is evident in Figure 2-1, approximation of the efficiency factors near a radius of 10^3 μm is quite difficult because of the change in the efficiency factor curve as it nears the asymptotic value. This problem is even more evident in Figure 2-2 for a wavelength of 5 cm where the efficiency factors vary in a highly complex fashion. It is not possible to simulate accurately such variability without using a full scattering treatment but it was felt that a better approximation could be developed by adding a fourth region for the radius sizes between the well fit transition region and the clearly asymptotic region.

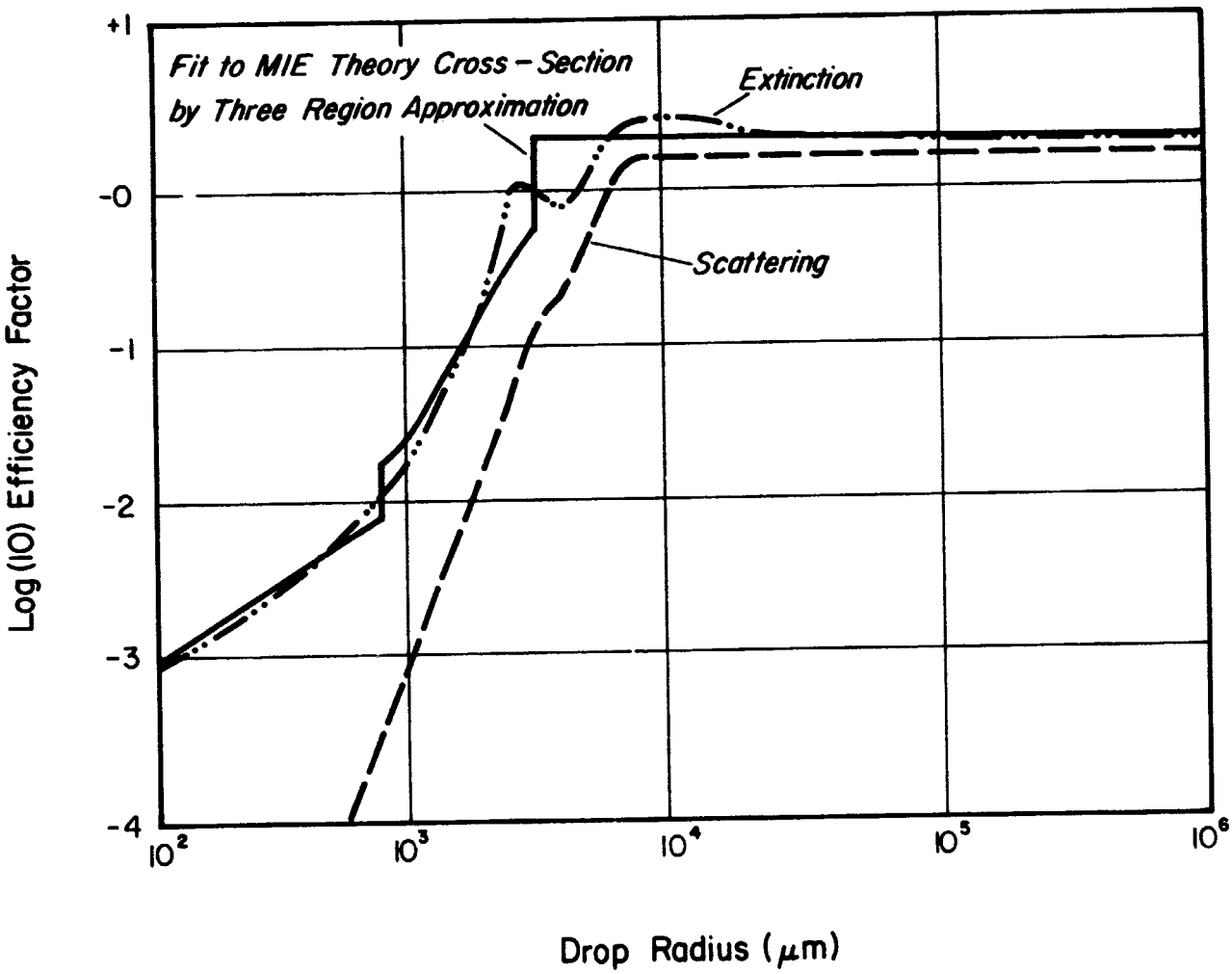

Figure 2-2 Fit to Mie Efficiency Factor at λ = 5.0 cm (6 GHz) and 298°K.

To permit an accurate computation of the Q_E values within the transition region, the approximation was split into its component terms.

$$Q_E = Q_A + Q_S$$
$$Q_A = qZ\ (\lambda,T) + q^3\ A\ (\lambda,T) \qquad (2\text{-}9)$$
$$Q_S = q^4\ B\ (\lambda,T)$$

where Q_A is the efficiency factor due to absorption, Q_S is the efficiency factor due to scattering and the other terms are as described above.

Figure 2-3 shows the fit of the approximation at a wavelength of 1.55 cm of these three efficiency factors to the values computed using the full Mie computation efficiency values generated by ERT's Mie scattering program (Gaut and Reifenstein, 1971). [In this figure $Q_E = Q(E)$, $Q_A = Q(A)$, $Q_S = Q(S)$]. In this figure r_{c_A} indicates the radius value (r_c) used in the approximation as the upper limit to the transition region and r_{c_S} shows the lower limit to the large sphere region in the exact calculations. The curve marked "Q_A and Q_E approximate" shows the extremely high efficiency values that would be computed if the transition region were continued to r_{c_S}. It is also apparent that the use of $Q_E = 2$ in the region of r_{c_A} to r_{c_S} overestimates the efficiency factors.

It is evident though that the use of an accurate fit to the Q_A value between r_{c_A} and r_{c_S} combined with the Q_S computation used in Region 2 would generate a good approximation to the Q_E value. This is not necessarily true at all wavelengths (e.g., see Figure 2-2) but is applicable to the wavelengths near 1 cm which are currently used to measure precipitation (e.g., 19.35 GHz and 37 GHz) and which are most sensitive to the occurrence and distribution of precipitation size drops. The approach described below was thus designed to provide a good approximation for these wavelengths and a reasonably good approximation at other wavelengths in the microwave region.

Using the data shown in Figure 2-3, the fourth approximation region was defined with the limits r_{c_A} and r_{c_S}. In this region, the following approximations were used:

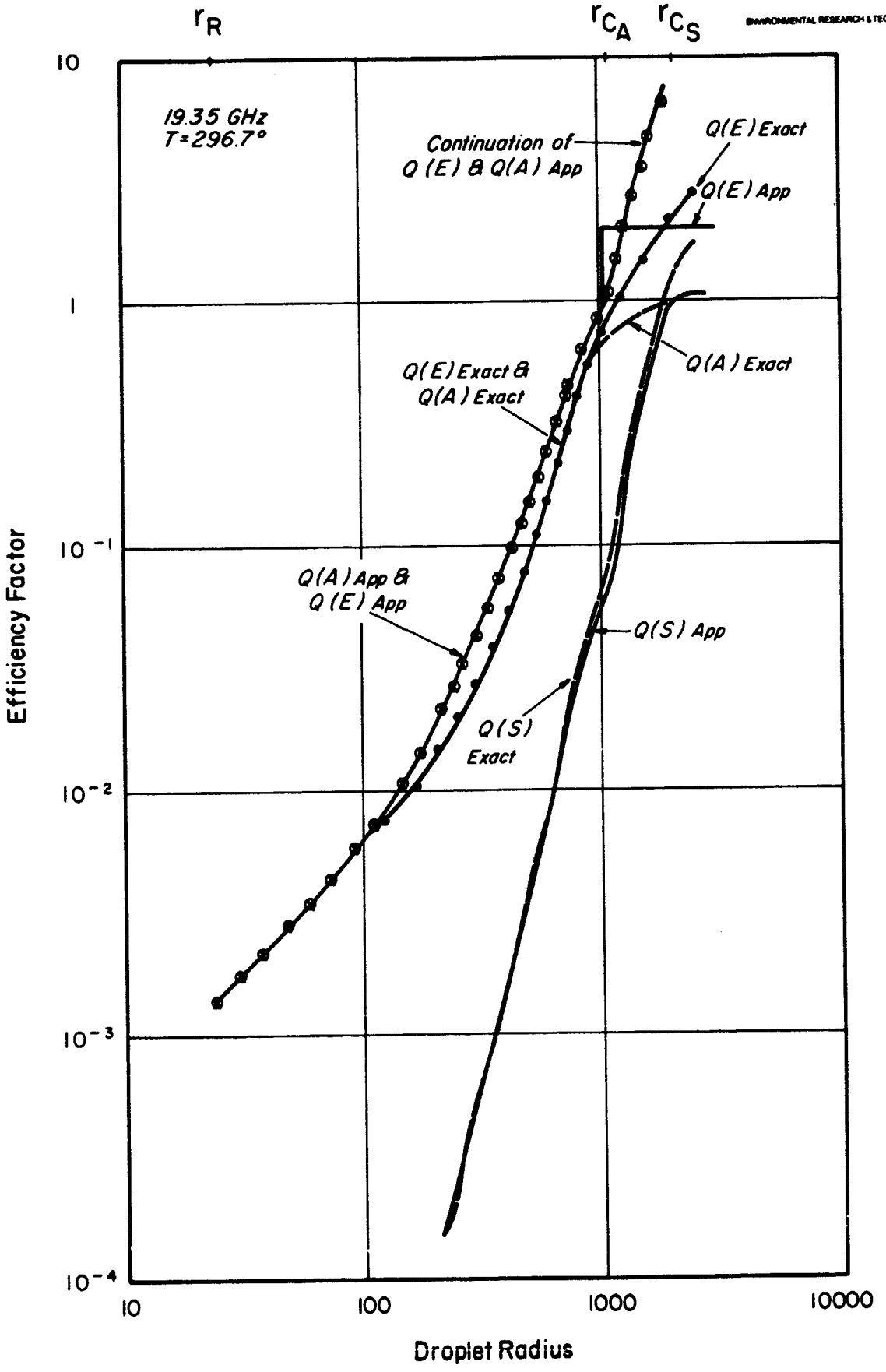

Figure 2-3 Fit to Mie Efficiency Factors at λ = 1.55 cm (19.35 GHz) and 296.7°K, Preliminary Approximation.

$$Q_A = Q_{A_{r_{c_A}}} + (1 - Q_{A_{r_{c_A}}}) \left(\frac{r - r_{c_A}}{r_{c_s} - r_{c_A}} \right)$$

$$Q_S = q^4 B (\lambda, T) \qquad (2\text{-}10)$$

where

$$Q_{A_{r_{c_A}}} = qZ (\lambda, T) + q^3 A (\lambda, T)$$

when

$$r = r_{c_A}$$

Q_A is thus specified by a linear function whose values increase from the absorption efficiency factor limit of the transition region to the absorption asymptotic factor of 1. This formulation does not derive from a series expansion of Mie efficiency factors but rather from a curve fit to the computed efficiency factors in this region. The approach used is thus semi-empirical, diverging somewhat from the purely theoretical approach initially used, but leading to a significant improvement in the overall approximation.

A related modification was made in the absorption approximation in the original transition region. Reexamination of Figure 2-3 showed that Q_A tended to be overestimated in this region leading to a corresponding error in Q_E especially for droplet radii where scattering effects are minimal. This can lead to significant errors in the extinction coefficient for wavelengths near 1 cm for the majority of precipitating droplets occur in this size region. An empirical function was thus designed to adjust the Q_A values leading to the following expression:

$$Q_A = qZ (\lambda, T) + (q^3 A (\lambda, T)/F(r))$$

where

$$F(r) = 3, \quad r \leq 0.15\, r_{c_A}$$

$$F(r) = 3.1 - 2.5 * \left(\frac{r - 0.1\, r_{c_A}}{r_{c_A}} \right),$$

$$0.15\, r_{c_A} \leq r \leq 0.75\, r_{c_A}$$

$$F(r) = 1.5, \quad 0.75\, r_{c_A} \leq r \leq r_{c_A}$$

It will be noted that this adjustment is not tied to particular wavelengths but rather is designed to apply to most of the microwave region.

The result of these two modifications are shown in Figures 2-4 and 2-5 representing efficiency factors at wavelengths of 1.55 and 0.8 cm and a temperature of 296.7°. The improvement in the approximation is clearly seen by a comparison of Figure 2-4 with Figure 2-3 while Figure 2-5 shows the applicability of the revised approximation at other wavelengths. Through these and other verification studies, the revised model was thus defined as:

$$Q_E = qZ, \qquad r < r_R \tag{2-11}$$

$$= qZ + A\, q^3/F(r) + B\, q^4, \quad r_R \leq r \leq r_{c_A} \tag{2-12}$$

$$= Q_{A_{r_{c_A}}} + (1 - Q_{A_{r_{c_A}}}) \frac{r - r_{c_A}}{r_{c_s} - r_{c_A}} + B\, q^4, \tag{2-13}$$

$$r_{c_A} < r < r_{c_s}$$

$$= 2, \qquad r_{c_s} < r \tag{2-14}$$

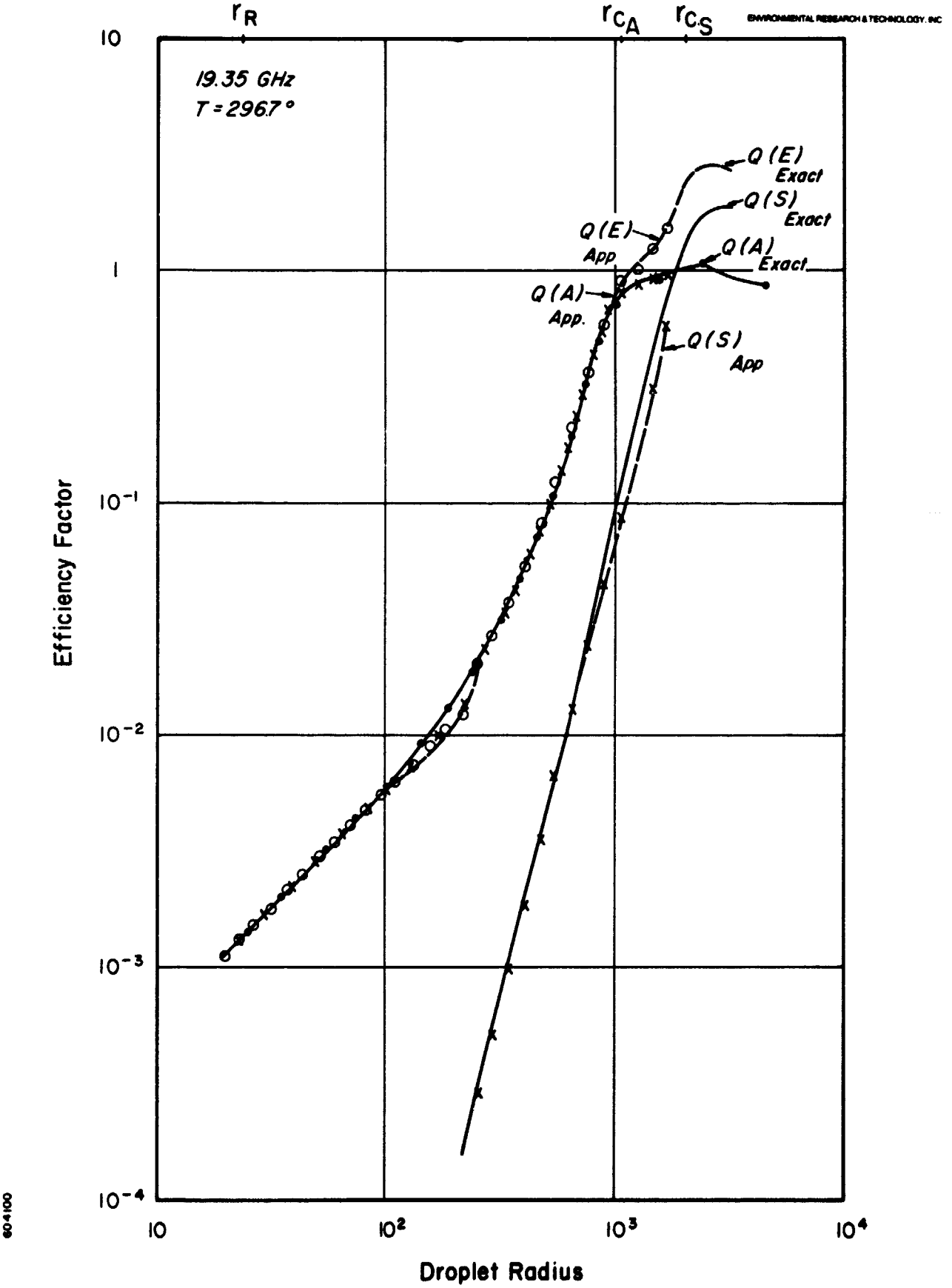

Figure 2-4 Fit of Mie Efficiency Factors at λ = 1.55 cm (19.35 GHz) and 296.7°K, Revised Approximation.

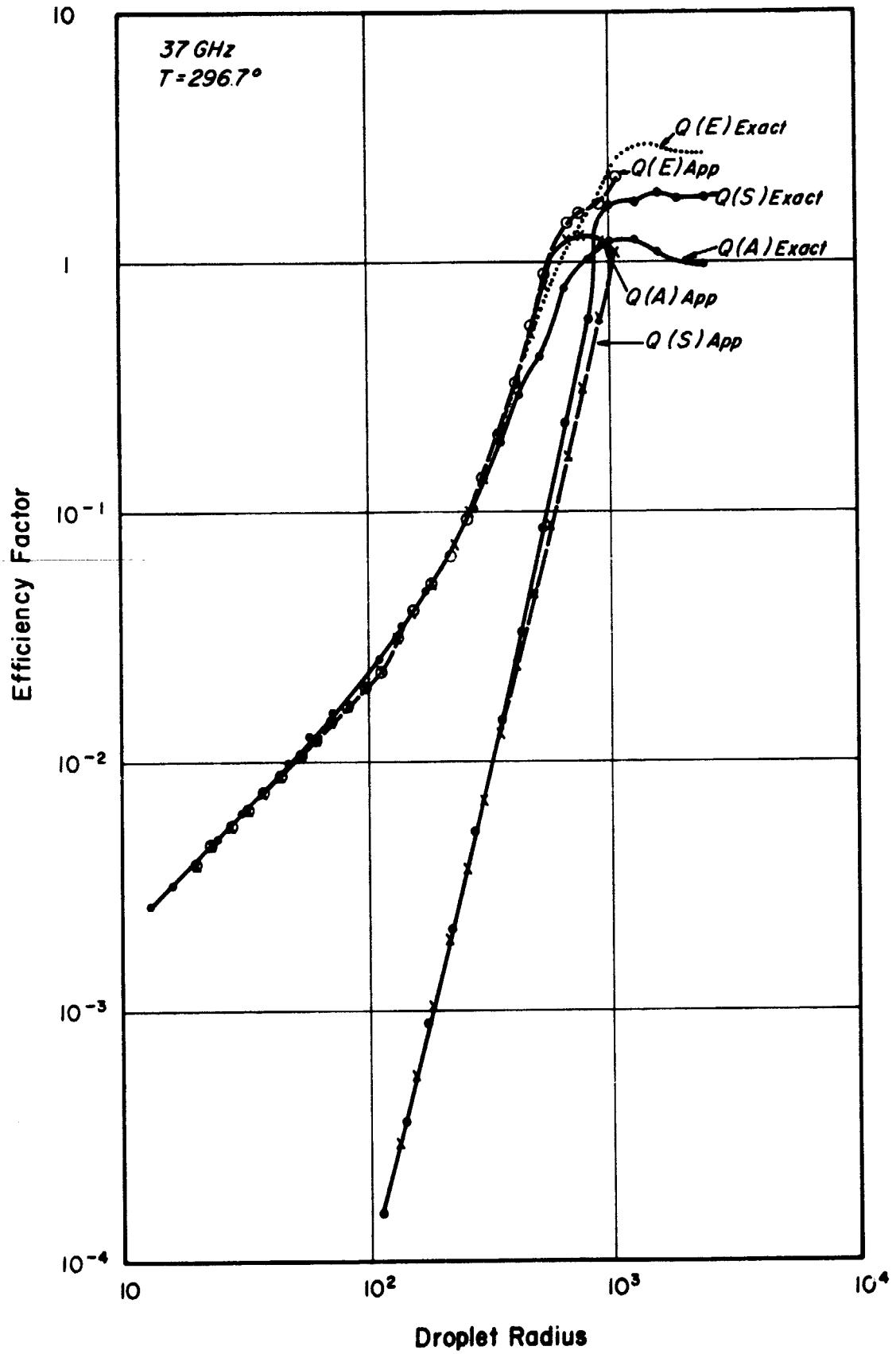

804048

Figure 2-5 Fit of Mie Efficiency Factors at λ = .81 cm (37 GHz) and 296.7°K, Revised Approximation.

which allows the expression shown in Equation 2-7 to be truncated to a series of four integrals:

$$\gamma_E \simeq \int_0^{r_e} qZ\, N(r)\, \pi r^2\, dr$$

$$+ \int_{r_R}^{r_{c_A}} (qZ + A\, q^3/F(r) + B\, q^4)\, N(r)\, \pi r^2\, dr$$

$$+ \int_{r_{c_A}}^{r_{c_S}} \left(Q_{A_{r_{c_A}}} + (1 - Q_{A_{r_{c_A}}}) \left(\frac{r - r_{c_A}}{r_{c_S} - r_{c_A}}\right) + B\, q^4\right) N(r)\, \pi r^2\, dr$$

$$+ \int_{r_c}^{\infty} 2\, N(r)\, \pi r^2\, dr \qquad (2\text{-}15)$$

where all terms are as previously defined.

2.5 Drop Size Distribution Function

In order to evaluate Equation 2-15, the drop size distribution must be specified. The particular form of the drop size distribution N(r) is empirically determined and for the purpose of our study, the most general specification for cloud droplet spectra is the Deirmendjian (1964) distribution:

$$N(r) = Ar^{C_1} \exp\{-Br^{C_2}\} \qquad (2\text{-}16)$$

which characterizes the distribution in terms of four parameters, two of which (A and B) are scale parameters, the others being shape parameters. Fair weather and stratus clouds conform nicely to this characterization. A simple form of the Deirmendjian distribution may be used to describe precipitation.

A review of the literature, especially that pertaining to radar studies of precipitation, indicated that the Marshall-Palmer (1948)

model of drop size distribution for precipitation is often used in studies of satellite-measured brightness temperatures. The virtues of this model are that: 1) an empirical expression exists which relates the drop size distribution (useful in computations of radiative interaction) to the instantaneous rainfall rate (useful in synoptic studies), and 2) the form of the expression is essentially that of the Deirmendjian expression used in modeling cloud droplet distributions. The Marshall-Palmer model is expressed as:

$$N(r,R) = k_1 \exp - \{k_2 \, rR^{-k_3}\} \tag{2-17}$$

where

$$k_1 = 16.0 \times 10^{-6}$$

$$k_2 = 8.156 \times 10^{-3}$$

$$k_3 = 0.21$$

and

N(r,R) is the number density of particles per unit size range (cm^{-3} μm^{1}).

r is the droplet radius (μm) for a given rain rate.

R is the rainfall rate (mm/hr).

This is essentially the Deirmendjian distribution with parameters:

$$A = k_1$$

$$B = k_2 R^{-k_3}$$

$$C_1 = 0$$

$$C_2 = 1$$

For the preliminary analysis of this approximation, the Marshall-Palmer distribution was incorporated into Equation 2-15. This was done not only because of the advantages outlined above, but also because it

permitted evaluation of the integrals in a closed form (when F(r) is ignored) and because it allowed comparison with results obtained in other studies using the full scattering treatment.

During this study the general Deirmendjian form was incorporated into the formulation for γ_E. Initially the integrals resulting from these spectra were evaluated in a closed form but this proved to limit severely the choice of spectra representing rain and to cause undue computational complexity.

The above integrals (assuming F(r) = 1) are all of the form:

$$\int r^n e^{-ar^x} dr \tag{2-18}$$

which may be integrated only when x = 1 and n is a positive integer. Such integration is done using the recurrence relation:

$$\int r^n e^{-ar} dx = \frac{-e^{-ar}}{a^{n+1}} \sum_{m=0}^{n} \frac{n! (ar)^{n-m}}{(n-m)!} \tag{2-19}$$

This relationship can be done simply and directly used for the M-P distribution where x equals 1 and n is always a positive integer (see Equations 2-15 and 2-17).

The Deirmendjian distribution represents a far more complex case. In Equation 2-16, C_1 and C_2 can assume a wide variety of values, many of which do not meet the above constraints. In fact the formulation generally requires a transformation of variables such that the integral becomes:

$$\frac{1}{C_2} \int r^{\frac{C_1 + m - C_2 + 1}{C_2}} e^{-ar} dr \tag{2-20}$$

where m=2 plus the appropriate power of q. This can be evaluated only when $(C_1 + m - C_2 + 1)/C_2$ is a positive integer and thus only for a very limited number of C_1, C_2 combinations. In turn, this restricts the types of precipitation cases which can be simulated and does not meet the study's goal of a generalized model. Furthermore for certain combinations of C_1 and C_2 which can be used (e.g., 6, 0.5) the number and size of the terms in the recurrence relationship can become exceedingly large leading to considerable computer processing time and possible computational errors due to roundoff.

An alternate approach to integration was thus adopted - use of a trapezoidal approximation instead of an analytic evaluation. This followed the technique used in the full computation of extinction by ERT (Gaut, and Reifenstein, 1971) dividing the droplet distribution by geometric progression into forty intervals for which the term to be integrated was evaluated. These evaluated terms were then summed to provided the desired extinction coefficient. This technique has several advantages in that 1) it is rapid, accurate and simple computationally, 2) it permits the ready incorporation of the F(r) correction to absorption, and 3) it allows the use of any C_1 and C_2 factors and is thus generally applicable.

The final ERT precipitation approximation thus consists of a series of integral terms which will represent the absorption, scattering and extinction due to cloud and raindrops. These terms can be used with any drop size distribution expressible in the Marshall-Palmer or Deirmendjian formulations making possible a realistic simulation of the majority of precipitation cases occurring on a seasonal or global basis. The utility of this approximation lies in its ability to provide layer extinction coefficients for any microwave frequency, atmospheric temperature and droplet configuration while avoiding the computational complexity of the full Mie solution.

2.6 Radiative Transfer Model

The equation of radiative transfer (Chandrasekhar, 1960) at a single frequency may be written

$$\frac{dT_B(\theta)}{dZ} + \gamma_E T_B(\theta) = \gamma_S \int_0^{\pi} (T_B(\theta_S) F(\theta,\theta_s) \sin \theta_s \, d\theta_s) + \gamma_A T(z) \quad (2\text{-}21)$$

where

$T_B(\theta)$ is the brightness temperature at polar angle θ.

θ_s is the scattering angle.

$F(\theta,\theta_s)$ is the scattering phase function.

Z is the ray path length.

$T(Z)$ is the atmospheric temperature and γ_E, γ_A and γ_S are the coefficients of extinction, absorption and scattering, respectively.

In Equation 2-21, the two terms on the left give the change in radiance in a given direction and the extinction of brightness temperature due to absorption and scattering away from a specified angle θ. The first term on the right expresses the increase in radiance in the direction θ due to scattering from other angles. The second term represents atmospheric thermal emission.

The exact solution to this equation may be found by first computing the approximate brightness temperatures by assuming no scattering and then iterating to use the computed layer T_B's with the scattering term (see Equation 2-21) to generate new T_B's. This procedure is repeated using the T_B's of the previous iteration until successful convergence is reached (e.g., see Wilheit, et. al., 1975).

This iterative approach, of course, requires an extensive number of computations and long data processing times, exactly the difficulties which this program wished to avoid. Thus a second approximation to rain effects was developed - an approximation to the radiative transfer equation. In this approximation it is assumed that there is no increase in radiance due to scattering such that Equation 2-21 becomes:

$$\frac{dT_B(\theta)}{dZ} + \gamma_E T_B(\theta) = \gamma_A T(z) \qquad (2\text{-}22)$$

This assumption is justified for most of the rain rates of interest here because

$$\gamma_S \int_0^{\pi} (T_B(\theta) F(\theta_1,\theta_S) \sin \theta_s \, d\theta_s) < \gamma_A T(z)$$

Only at very high single scattering albedoes ($\gamma_S/\gamma_E > 0.5$) will this cause a significant error but these correspond to very high rain rates whose probability of occurrence is low and which cause saturation in microwave emission values.

The final approach to determining the effects of precipitation on microwave radiation thus does not specifically treat all effects of scattering by raindrops. Rather it approximates the total emission due to precipitation. As the results below will show, this technique permits a realistic assessment of rain effects.

2.7 The Verification of the ERT Precipitation Model

During the development and evolution of these approximations, considerable effort was spent in comparing the model results with results derived through the use of exact Mie and radiative transfer calculations. The preliminary Marshall-Palmer model results showed good agreement in its extinction coefficients with those presented by Shifrin and Chernyak (1970) which were calculated from Mie theory for a number of wavelengths. Differences between the two sources were further decreased when the fourth region and the absorption correction were incorporated. The extinction coefficients due to two different Deirmendjian distributions were compared with those calculated by ERT's single scattering model at a number of atmospheric temperatures for a wavelength of 1.55 cm and indicate that, while some differences still exist, the approximation is very good.

Finally for a complete test of the entire model, the brightness temperatures computed using the ERT approach were compared with those derived from the full scattering treatment used by Wilheit, et. al. (1975). Both of these sets of values represent a 4 kilometer thick uniform rain cloud imbedded in a tropical atmosphere over a calm sea at 300°. The drop size distributions in these cases were represented by the Marshall-Palmer function. The atmospheric models differed slightly in the structure of atmospheric temperature and in the cloud top temperature (273° Wilheit, 275° ERT) but these should cause only minor differences in the total radiance sensed. Figure 2-6 shows the values simulated by both models when only absorption is assumed and when absorption plus scattering is encountered. (In the pure absorption case, $\gamma_E = \gamma_A$ in Equation 2-22). The absorption curves are provided only as a guideline to the effects of scattering and are not meant to be used as a microwave rain rate relationship.

Up to 10 mm/hr, both curves show that inferred rain rates using ERT's approach would be in error by only 1 mm/hr. This agreement is excellent, especially since none of the approximations made in this study were based upon or tailored to the radiometric models used by Wilheit, et. al. (1975). Beyond 10 mm/hr the system shows slightly larger errors due primarily to the higher cloud top temperature in ERT's atmospheric model and to a slightly higher absorption coefficient in the ERT model. Despite this, both models are in good agreement on the amount of rain needed to saturate the radiometric measurements and the brightness temperatures associated with saturation.

2.8 Summary

ERT has developed a generalized precipitation model which permits the determination of the effects of precipitation on microwave radiation. This model, using both an approximation to the hydrometeor extinction coefficient and an approximation to the equation of radiative transfer, does not attempt to treat precisely the effects of scattering by rain drops but rather simulates the extinction of radiation in the presence of precipitation. The results shown above indicate that this approach is valid. Section 4 will apply this model to analyze the effects of varying cloud microstructure and macrostructure on radiometric measurements.

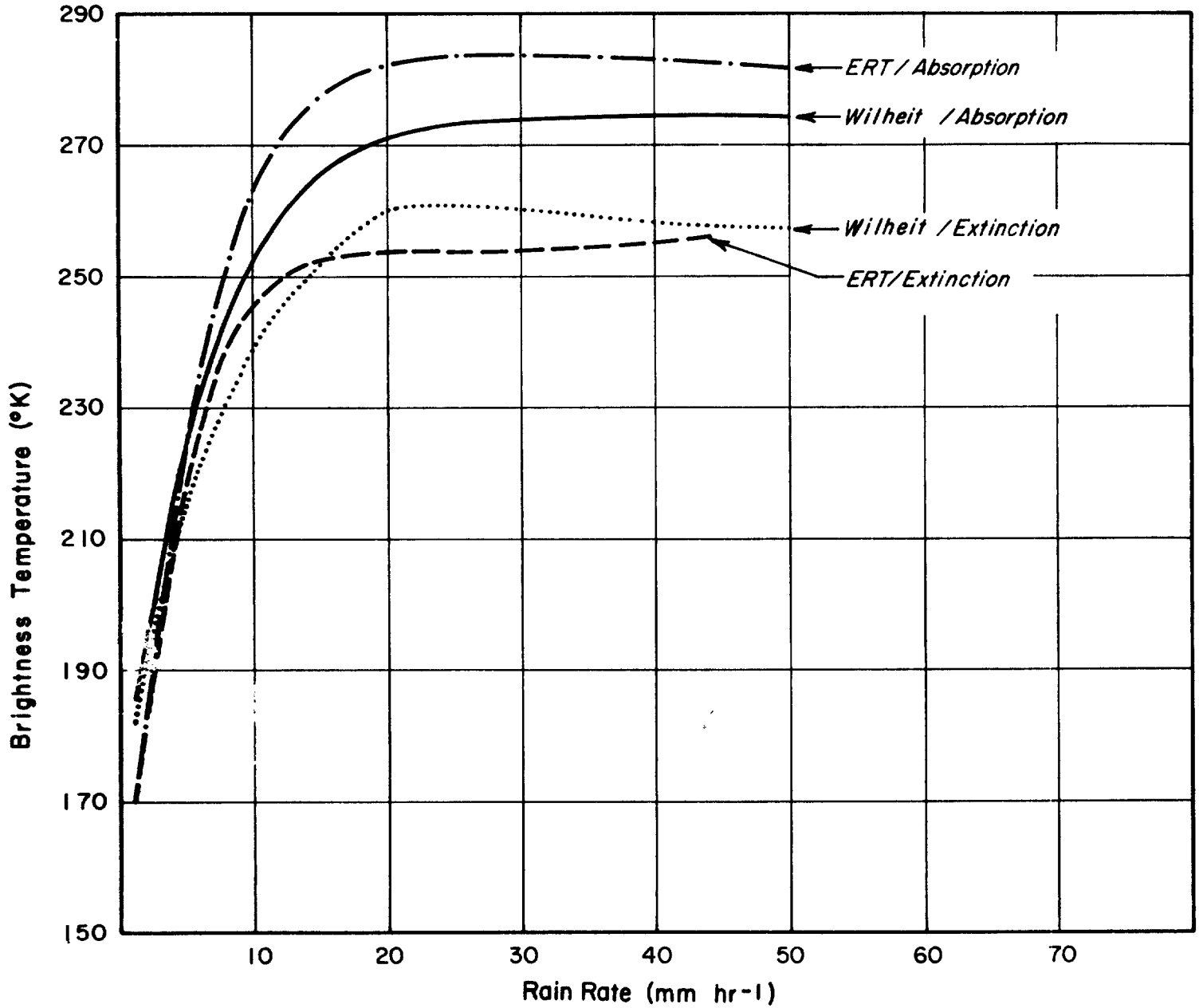

Figure 2-6 Comparison of Brightness Temperatures Computed from Full Mie Scattering Theory (Wilheit et al, 1975) and the ERT Model for a 4 km Uniform Marshall-Palmer Tropical Cloud.

3. THE INFERENCE OF RAIN RATES FROM MICROWAVE MEASUREMENTS

The determination of precipitation rates from radiometric measurements requires an understanding not only of the physical processes relating hydrometers and microwave radiation, but also of the natural structure and variability of the hydrometers and the atmosphere in which they occur. As the previous section demonstrated, a radiometric model has been developed which accurately simulates the effects of precipitation on microwave radiation. This section will discuss the characteristics of precipitation itself and the meteorological models of precipitation which would be used in the simulation of microwave measurements.

3.1 The Inversion of Radiometric Measurement

Inversion of geophysical parameters from radiometric data has been the focus of a large number of studies and technique development. In the approach used by ERT, a statistical inversion procedure has been developed which relies upon the correlation of atmospheric and surface parameters with measured microwave emissions. This procedure, shown in Figure 3-1, has been discussed in a number of reports (e.g., Gaut and Reifenstein, 1970, 1971; Reifenstein and Gaut, 1971; Gaut, et. al., 1972, 1974; Willand, et. al., 1973, Fowler, et. al., 1975) so only a brief summary will be provided here.

As shown in Figure 3-1, the primary data input to the statistical inversion procedure consists of geophysical models and their associated probability of occurrence. The atmospheric temperature, pressure, and water vapor profiles for these models are provided by daily radiosonde measurements made at selected locations over a multi-year period. Since radiosonde data do not contain cloud measurements, these soundings are supplemented by a set of cloud models corresponding to the season and region under analysis. The probability of occurrence of these models is derived from the global cloud statistics data base (Chang and Willand, 1972) and is used with a random number generator to insert the proper distribution of cloud types into the atmospheric soundings. Finally

statistics of the background, such as the mean and standard deviation of temperature, surface wind speed, and salinity of the ocean, are specified through the use of climatological data and used to define the surface characteristics associated with each atmosphere.

The resulting geophysical models are then input to the radiometric interaction model which simulates the brightness temperatures for each microwave channels under analysis. These radiometric values are then correlated with the geophysical parameters given in the initial atmospheric and surface models to generate a "D-matrix". In the actual inversion procedure, simulated or measured brightness temperatures are input to the D-matrix to infer the conditions which they represent.

In the previous studies cited above, this procedure has been used to infer a variety of parameters such as atmospheric temperature profiles, integrated water vapor and liquid water and surface wind speed over the oceans. These are parameters whose characteristics and effects on microwave radiation are well defined and thus inversion of these parameters has been quite successful.

Precipitation, on the other hand, is a far more difficult parameter to estimate. For one thing, the interaction of rain drops with microwave radiation is a highly complex phenomenon for which simple simulation models have not been available. For another, precipitation characteristics have not been systematically observed and measured except in terms of rain rate. However, rain rate is not a parameter directly sensed by microwave radiometers; instead, radiometers are sensitive to the drop sizes and their number density which occur in the atmosphere. Thus, it is difficult to use standard meteorological observations in the statistical procedure.

Section 2 demonstrated that the first difficulty in measuring precipitation has been resolved through the development of an approximation to extinction which can be used directly in the radiometric model. The second difficulty, that of defining representative models of precipitating clouds, will be discussed here. Since precipitation is associated with certain cloud types such as cumulonimbus or nimbostratus, whose probability of occurrence is given in the cloud statistics of Chang and Willand (1972), and since observations of rain rate can be readily

converted to similar probabilities of precipitation amounts, no emphasis was placed upon the statistical aspects of precipitation. Rather, this study concentrated on the development of precipitating cloud models and the relationship of the microstructure to the commonly observed parameter, rain rate.

3.2 The Precipitating Cloud Models

As shown by Equations 2-1 and 2-21, the radiometric brightness temperature is a function of the atmospheric temperature and the drop-size distribution. In operational programs, the drop-size distribution is seldom known nor is it required as an output. Instead it is customary to relate the brightness temperature to a parameter of synoptic interest such as the rainfall rate at the surface. A difficulty arises because even at the earth's surface, there are many dropsize distributions which lead to the same rainfall rate; above the surface, the existence of strong vertical air currents can render the concept of a precipitation flux to be almost meaningless. Nevertheless, one objective of this study is to determine the effect of the drop-size distribution on the brightness temperature, where the results will be presented in terms of the rainfall rate calculated from various drop-size distributions using the terminal velocity values given for still air by Gunn and Kinzer (1949).

Drop-size distributions in rain have been measured for decades in a variety of storm types and climates. Generally the distributions have been obtained from direct sensors at the surface, but distributions aloft have also been deduced from an interpretation of the velocity spectra obtained with a vertically pointing Doppler radar. Battan (1973) has tabulated a large number of the measurement programs and has included the regression equations between rainfall rate and the radar reflectivity factor which is proportional to the sixth moment of the drop radius. Since rainfall rate is proportional to a factor between the third and fourth moment of drop radius, much of the variability given by Battan is a result of various size distributions in different types of rainfall. For example, the large number of small drops in orographic rain the tropics can lead to relatively high water contents and low precipitation rates compared to the leading edge of heavy

showers in which the distribution is characterized by relatively low water contents and high rain rates.

Only a few direct measurements of the drop-size distribution with height have been obtained. The best technique is to place a series of drop size spectrometers at various heights along the slope of a mountain as was done by Joss (private communication, 1976) and by Ohtake (1969). Some of the factors which can affect the drop-size distribution with height are growth by accretion and coalescence, drop break-up of large unstable drops, evaporation from the drops in unsaturated air, and the natural sorting of the drops by vertical wind shear. Some of these factors have been investigated theoretically by Rigley, et. al. (1954), Mason and Ramanadham (1954), and Hardy (1963). More recently, the modeling of processes within clouds has included the development of the cloud and precipitation distributions as a function of time (Young, 1975).

Radar has been used to investigate the variation of the radar reflectivity with height; Battan (1973) has summarized some of these studies. Generally, the results of radar observations indicate that for low melting level heights, relatively small changes take place in the drop size distribution below the melting layer of widespread precipitation. However, for high melting level heights, distribution changes may take place as indicated by the significant changes of reflectivity with height observed by Crane (1972). It should be noted that convective elements are nearly always present in widespread rain.

Radar observations of convective storms readily reveal the large changes in the storm structure over very small distances (Battan, 1973). These changes in radar structure are caused by variability in liquid water content and drop-size distribution, and because the structure is complex, it is exceedingly difficult to model in a manageable form.

In addition to the identifiable physical processes which can influence the drop-size distribution, the actual measurement of the distribution is a difficult task. Often the distributions are measured over volumes which are too small to provide a statistically meaningful sample, especially for the important larger size categories. Instrumentation errors, sometimes of unknown magnitude, are also present with some devices. At least some of the variability in the relationships

given by Battan (1973) is caused by the inability of present instruments to measure the distributions which are representative of relatively large volumes.

Despite the known large variability of drop-size distributions which can exist in the atmosphere, the experimental distribution formulated by Marshall and Palmer (1948) has been found to provide a useful guide for specifying the mean rain-drop distributions in widespread stratiform storms. As shown by Equation 2-17, the Marshall-Palmer distribution is a special case of the Deirmendjian distribution which is given in Equation 2-16 as

$$N(r) = Ar^{C_1} \exp\{-Br^{C_2}\}$$

where

$$A = m\, C_2\, B^{(C_1+4)/C_2} \Big/ \frac{4}{3}\, \pi\, 10^6\, r^{(C_1+4)/C_2}$$

$$B = C_1/C_2\, r_o^{C_2}$$

where

m is the mass density or liquid water content.

r_o is the mode radius.

C_1 and C_2 are two shape parameters which essentially determine how rapidly the number concentration decreases on the left and right respectively of the mode radius. In these shape parameters increases in C_1 and decreases in C_2 correspond to broadening in the spectra. The parameters A, B, C_1, and C_2 for the Marshall-Palmer distribution are given in Section 2. By specifying the four parameters in the Deirmendjian distribution, it is possible to generate the entire range of the physically realistic distributions which occur naturally.

Figure 3-2 shows the range of distributions which were used in one series of brightness temperature computations in a rain rate of about 9 mm hr^{-1}. The straight line is the Marshall-Palmer distribution which can be considered to be a rough guide for some types of rain. The distribution with a mode radius at 0.25 mm is much steeper than the Marshall-Palmer distribution whereas the other curve has a flatter slope. These

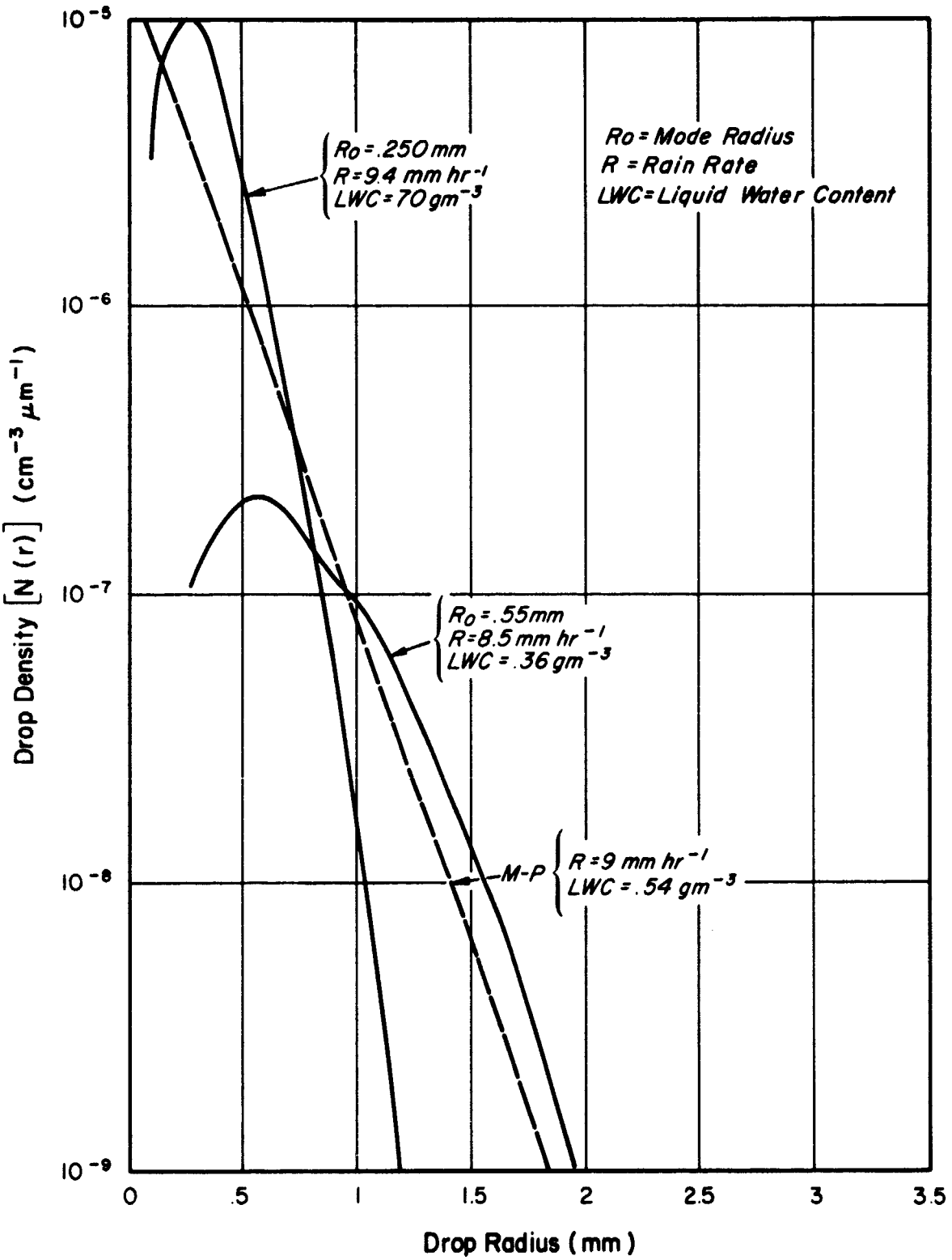

Figure 3-2 Selected Drop Size Spectra Corresponding to a Rain Rate of 9 mm hr^{-1}.

two curves represent the outside limits for distribution having a rain rate about 9 mm hr^{-1}. Note that the liquid water contents vary by almost a factor of two while the rainfall rates are within a range of ten percent. The brightness temperatures resulting from these distributions through certain layers of the atmosphere will be presented in Section 4.

Figure 3-3 shows the liquid water content and rain rate relationships for various Deirmendjian distributions which are defined by the indicated mode radii. In general, the shape factors were fairly similar and resulted in quite reasonable distributions. Also shown in the figure are the relationships derived from measured drop-size distributions in orographic rain in Hawaii, in showers, and in stratiform rain. The observed distributions fall generally within the mode radii limits of 200 and 450 μm; this information provided a guide for specifying the mode radii profile for the six models used for brightness temperature computations.

Because of growth processes or evaporation, the distribution shifts from predominantly small drops to larger ones as precipitation develops downward in a cloud (Hardy, 1963). At low rain rates, this shift was inferred from observations reported by Joss, et. al. (1974). An exception to this occurs when drops break up as a result of large melting ice or snow particles in heavy showers or at the melting layer in stratiform precipitation (Joss, private communication, 1976). However, for a representation of average precipitation models, it is reasonable to specify that the drop-size distribution shifts to larger drops and broadens as the precipitation approaches the surface. The shift of the mode radius with height is indicated in Figure 3-3 for a heavy tropical shower and for orographic rain. The shower model is characterized by a relatively large mode radius near the surface and a much smaller one at a height of 9 km. For the orographic model, the rain develops over a much shallower depth and has a relatively small mode radius.

In order to represent the variety of precipitation which can occur, six different models were specified as given in Table 3-1. The models were defined by the drop-size distribution and the mean temperature within one to five layers containing liquid precipitation. The appropriate standard atmosphere was used in all cases to specify the mean

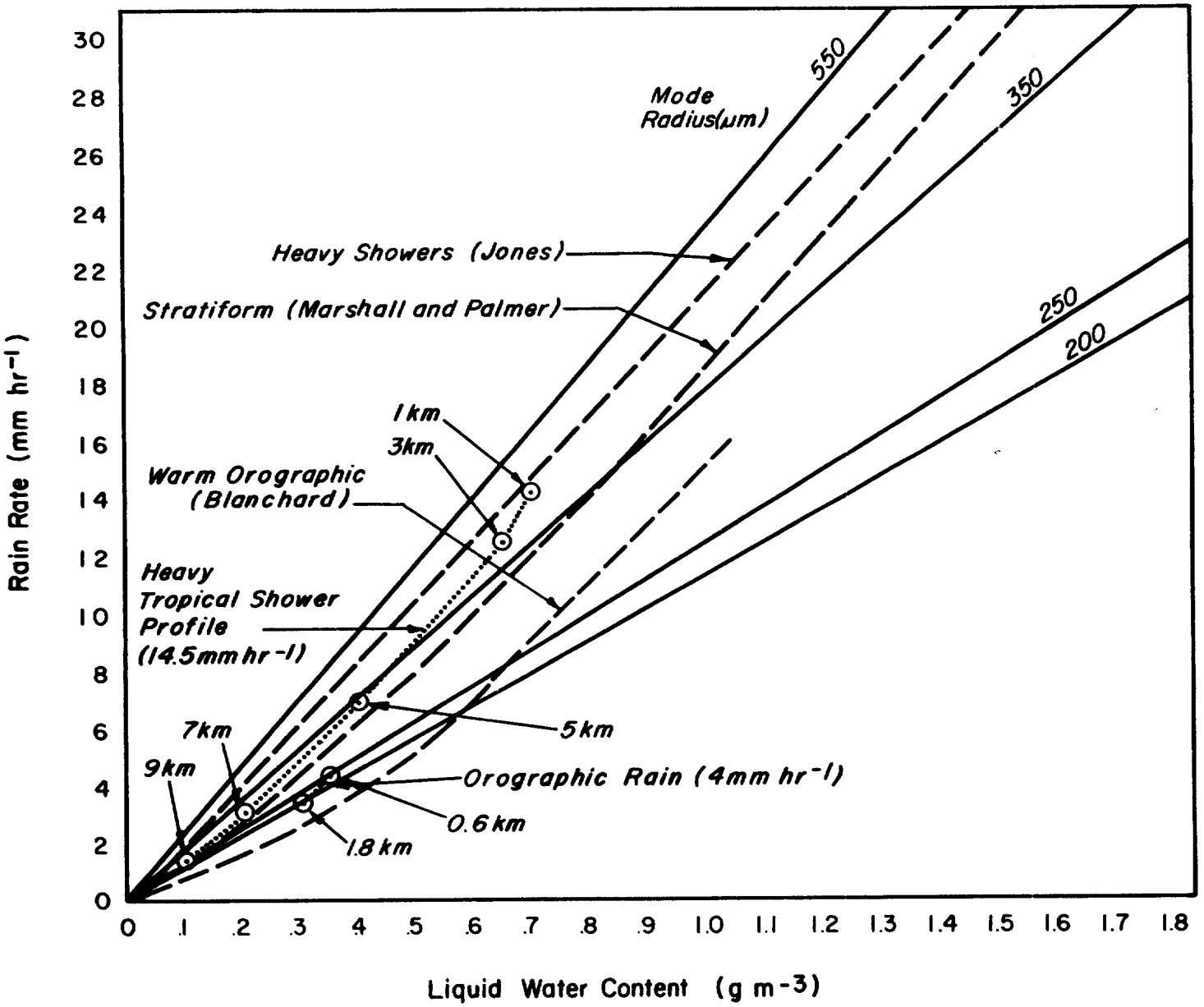

Figure 3-3 The Relationship Between Liquid Water Content and Rain Rate for Representative Drop Size Spectra.

TABLE 3-1

TEMPERATURE AND MODE RADIUS FOR EACH LAYER OF THE MODELS USED IN BRIGHTNESS TEMPERATURE COMPUTATIONS

(1) Heavy Tropical Showers (Some Water-Coated Ice)

2 km Layer Thickness

Mean Height (km)	C_1	C_2	Layer Mean Temp. (°K)	Mode Radius (μm)
1	4	1	298	450
3	6	1	284	400
5	6	1	270	350
7	6	1	258	300
9	6	1	246	200

(2) Warm Tropical Showers

2 km Layer Thickness

Mean Height (km)	C_1	C_2	Layer Mean Temp. (°K)	Mode Radius (μm)
1	4	1	298	450
3	6	1	284	400
5	6	2	270	350

(3) Widespread Rain: Midlatitude in Summer

2 km Layer Thickness

Mean Height (km)	C_1	C_2	Layer Mean Temp. (°K)	Mode Radius (μm)
1	4	0.8	291	380
3	4	1	280	340

(4) Widespread Rain: Midlatitude Spring and Fall

1.2 km Layer Thickness

Mean Height (km)	C_1	C_2	Layer Mean Temp. (°K)	Mode Radius (μm)
0.6	4	0.8	284	380
1.8	4	1	276	340

(5) Widespread Rain: Midlatitude in Winter and Arctic in Summer

1.5 km Layer Thickness

Mean Height (km)	C_1	C_2	Layer Mean Temp. (°K)	Mode Radius (μm)
0.75	4	0.8	277	355

(6) Orographic Rain: Midlatitude

1.2 km Layer Thickness

Mean Height (km)	C_1	C_2	Layer Mean Temp. (°K)	Mode Radius (μm)
0.6	5	1	284	250
1.8	6	1	276	200

temperature of the layer for the season and latitude considered. The drop-size distribution was generated by specifying the mode radius, the liquid water content and the two shape parameters of the Deirmendjian distribution. All parameters within the layer are assumed to be constant for a particular computation. Two tropical models are assumed; one is for rain produced by clouds which do not contain any ice, the other is for a much deeper cloud which contains ice. For the ice cloud, it is assumed that the particles are water coated and consequently might be approximated by water particles for the microwave wavelength of interest. This tropical cloud would be the worst case for extinction of the microwave energy. Models 3, 4 and 5 are for widespread rain in mid-latitudes for various seasons. Generally the rain for these models would originate from melting snow or ice although it is well known that widespread rain is often characterized by embedded heavy showers within the storm system. The last model represents the orographic heavy drizzle type rain which may occur over some parts of the world.

3.3 Spatial Variability

The models described in the above section are one-dimensional and describe the average rain environment over the beam width of a radiometric system. With satellite-borne radiometers, the beam integrates over large horizontal areas, and at this scale, the effect of the drop-size variability is likely to be small. Moreover, the equivalent rain rates for large areas rarely exceed 10 mm hr^{-1}. On the other hand, if measurements are obtained from aircraft-borne radiometers, the small-scale storm structure will be reflected in the observed rapid changes in observed brightness temperatures.

4. THE RELATIONSHIP BETWEEN RAIN RATE AND BRIGHTNESS TEMPERATURE

The radiometric precipitation model and the precipitating cloud models defined above permit a ready assessment of the effects of precipitation on microwave radiation. The cloud models and their associated atmospheres represent the diversity of rain conditions found on a regional and seasonal basis, and thus comparison of the brightness temperatures generated from these models provides a good analysis of the expected variability in the microwave-rain rate relationship. This analysis is necessary to determine the sensitivity of microwave sensors to rain and the feasibility of using such sensors in an operational mode to infer precipitation amounts.

During this study such an analysis was performed for the microwave frequencies of 19.35 GHz and 37 GHz (1.55 cm and 0.81 cm, respectively). The 19.35 GHz is well suited for precipitation studies because it has a strong, well-defined response to that atmospheric parameter (Wilheit, et. al., 1975), and measurements made at that frequency from the Nimbus 5 satellite have been used to detect rain. The 37 GHz channel, currently flown on Nimbus 6, also responds to precipitation although it is less suited to the discrimination of rain rates. Due to the differing responses at these frequencies, they make an excellent evaluation case and, since they are operational systems, the results of such an evaluation can be readily applied.

4.1 Analysis of Representative Precipitation Conditions

The six atmospheres and rain models specified in Table 3-1 represent convective and stratiform rain situations found in the tropics, midlatitudes and arctic. These cases were simulated through the use of ERT's radiometric model to determine the relationship between rain rate and brightness temperature for zenith viewing radiometers at 19.35 and 37 GHz. The results of this simulation for the 19.35 GHz channel are shown in Figures 4-1 through 4-6.

Figures 4-1 and 4-2 show the microwave response (absorption only and total extinction) to light tropical showers and heavy tropical thunderstorms, respectively, with the same atmosphere and surface used

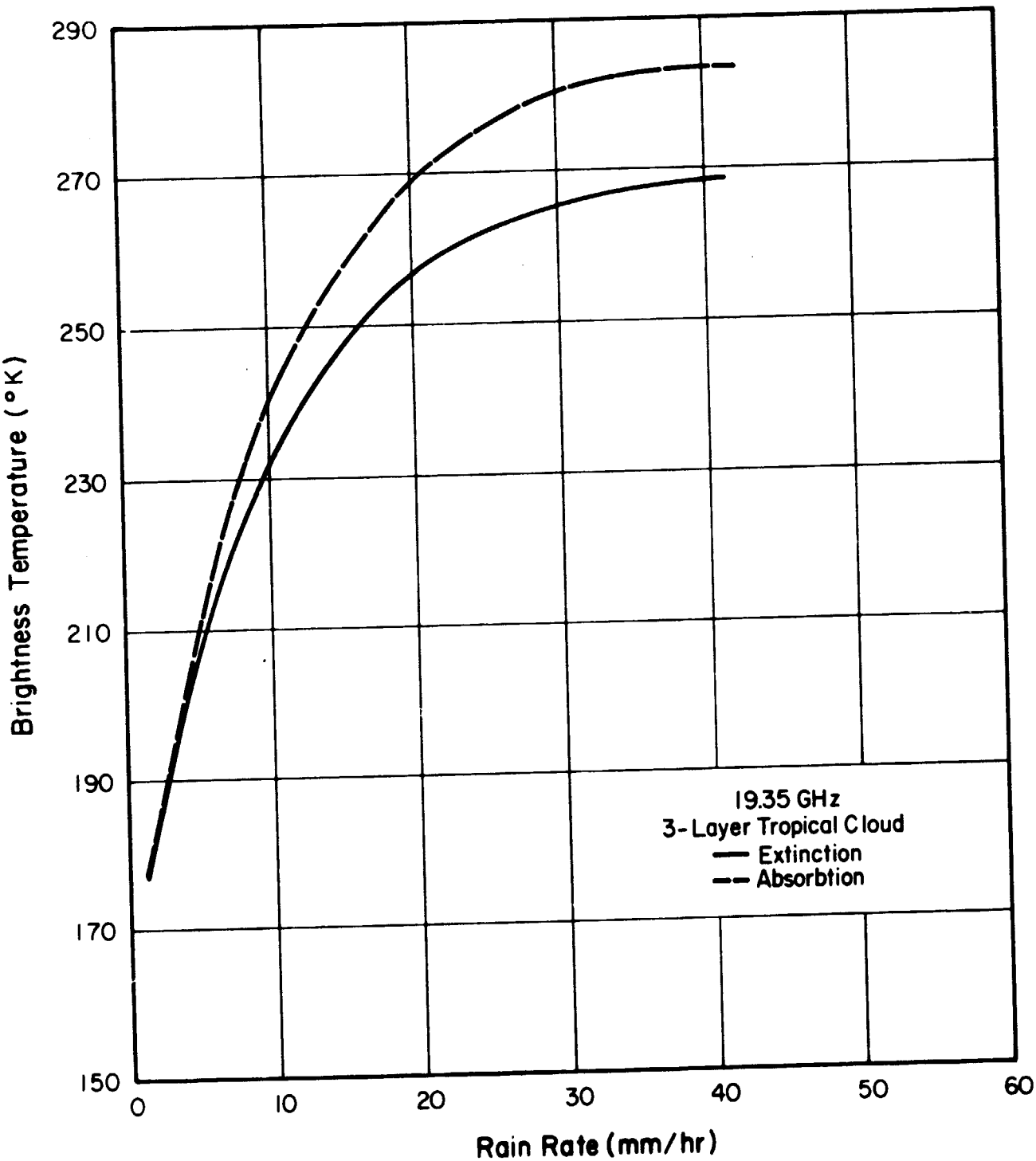

Figure 4-1 The Relationship Between Brightness Temperature and Rain Rate at 19.35 GHz for a Tropical Shower.

604030
604033

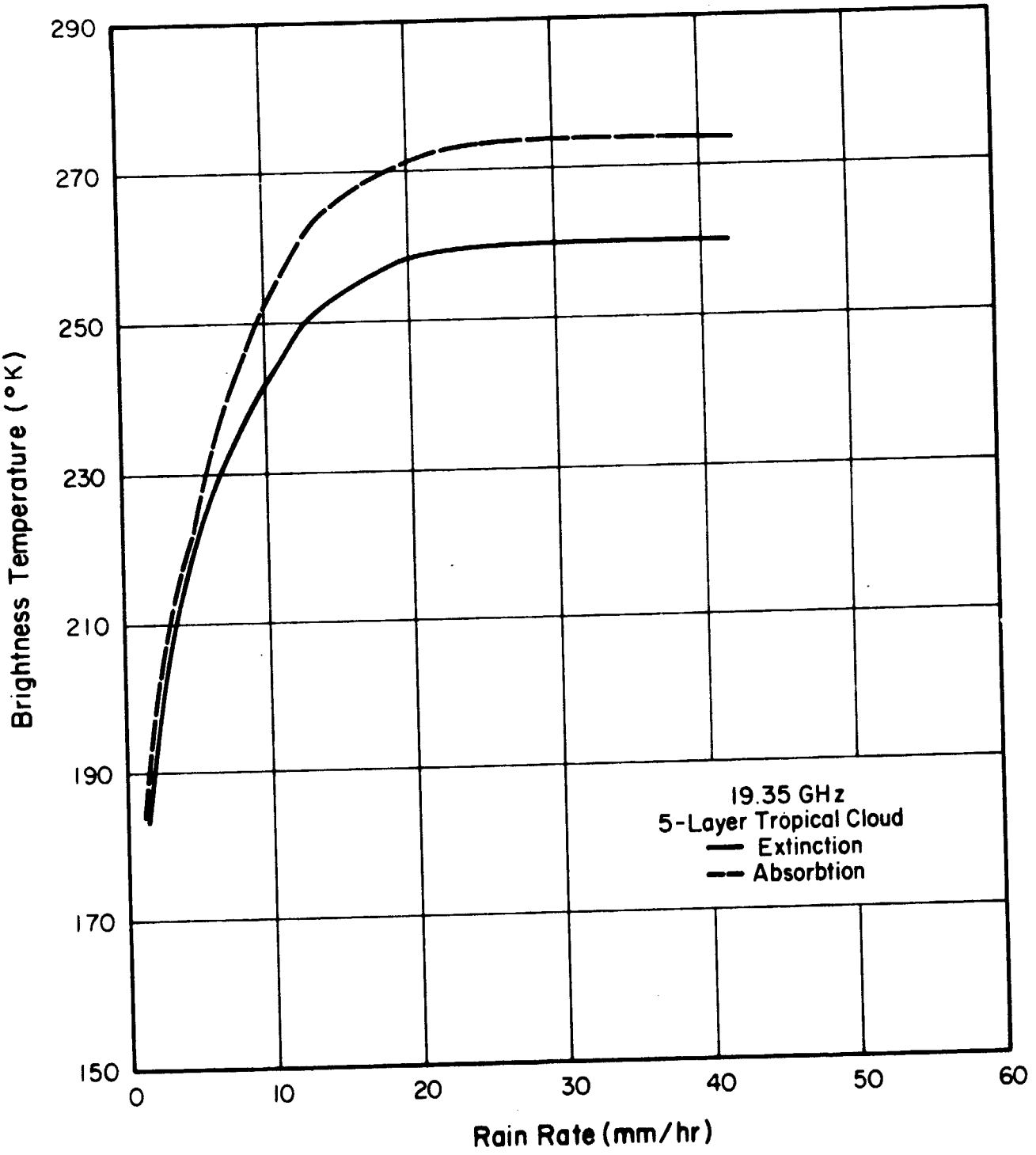

Figure 4-2 The Relationship Between Brightness Temperature and Rain Rate at 19.35 GHz for a Tropical Cumulonimbus.

604030
604031

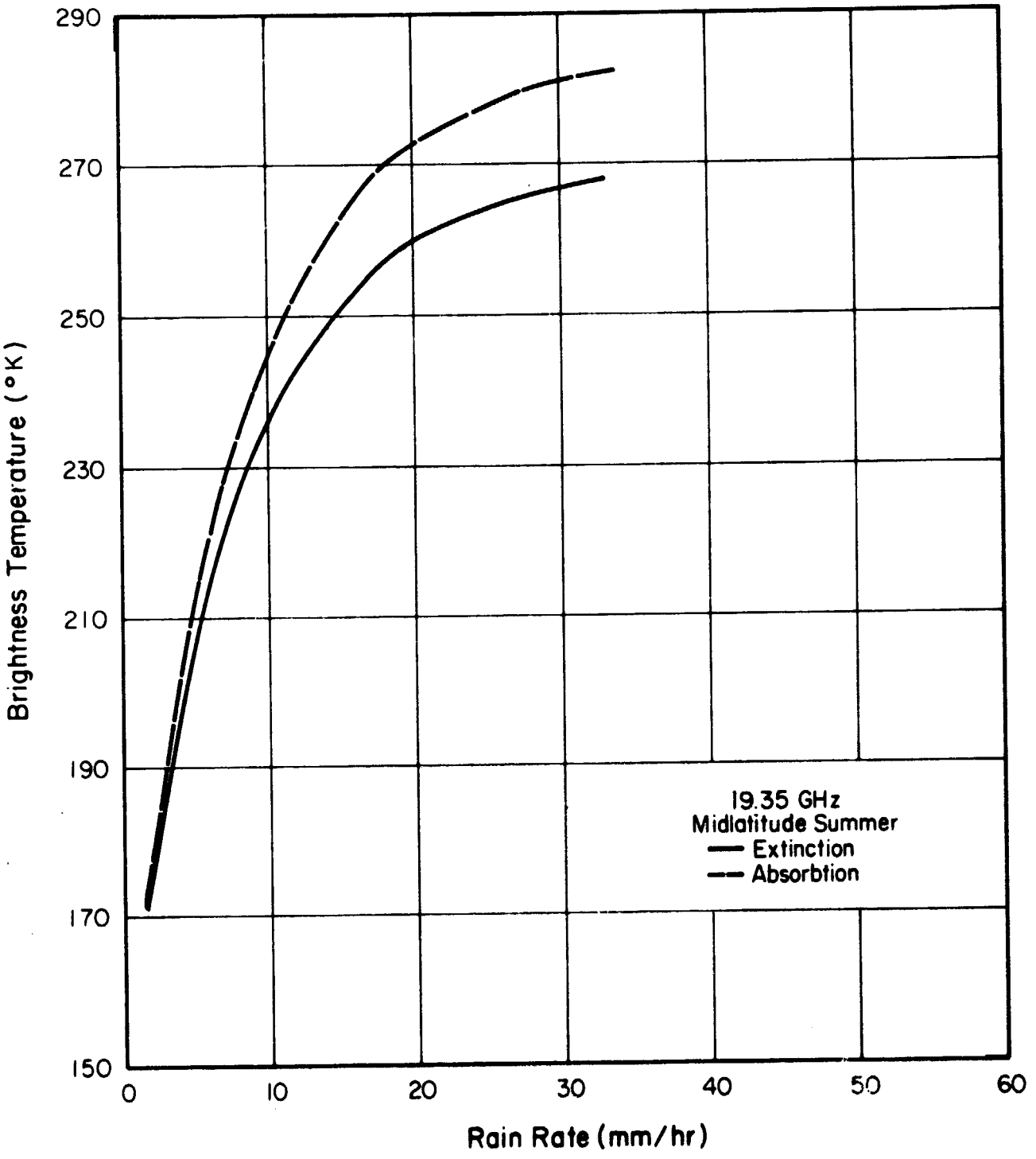

Figure 4-3 The Relationship Between Brightness Temperature and Rain Rate at 19.35 GHz for Midlatitude Summer Stratus.

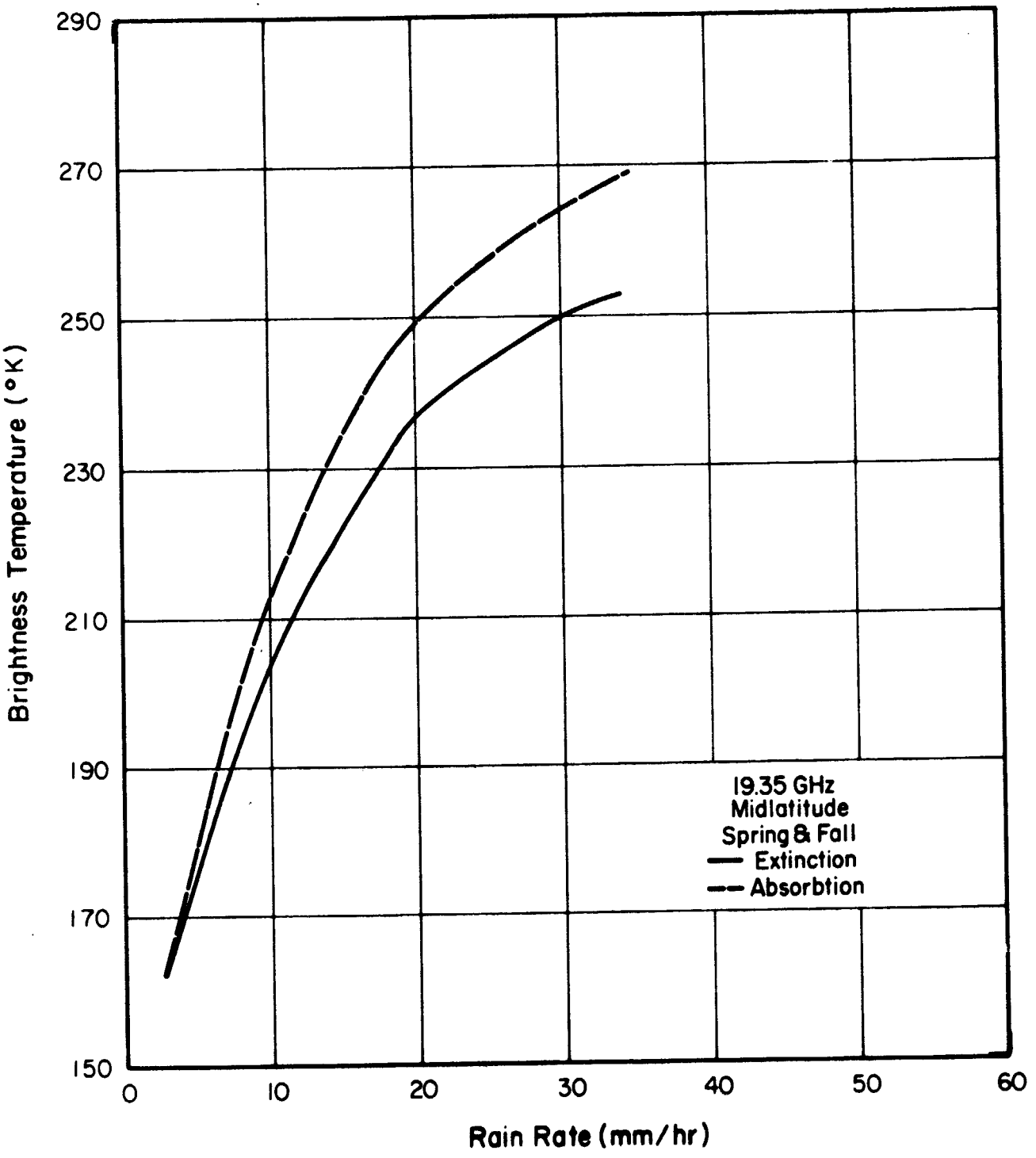

Figure 4-4 The Relationship Between Brightness Temperature and Rain Rate at 19.35 GHz for Midlatitude Spring/Fall Stratus.

604030
604036

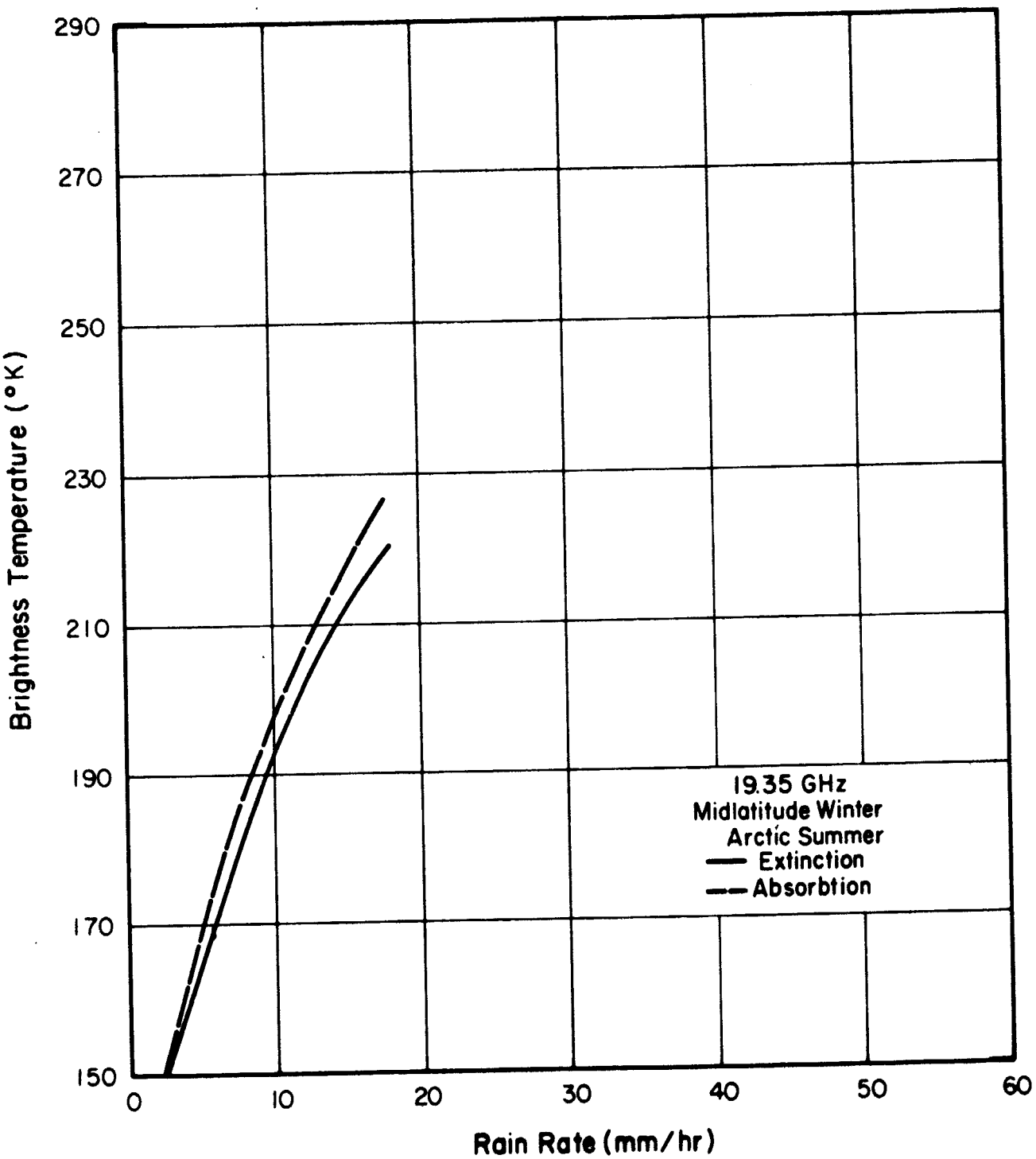

Figure 4-5 The Relationship Between Brightness Temperature and Rain Rate at 19.35 GHz for Midlatitude Winter Stratus.

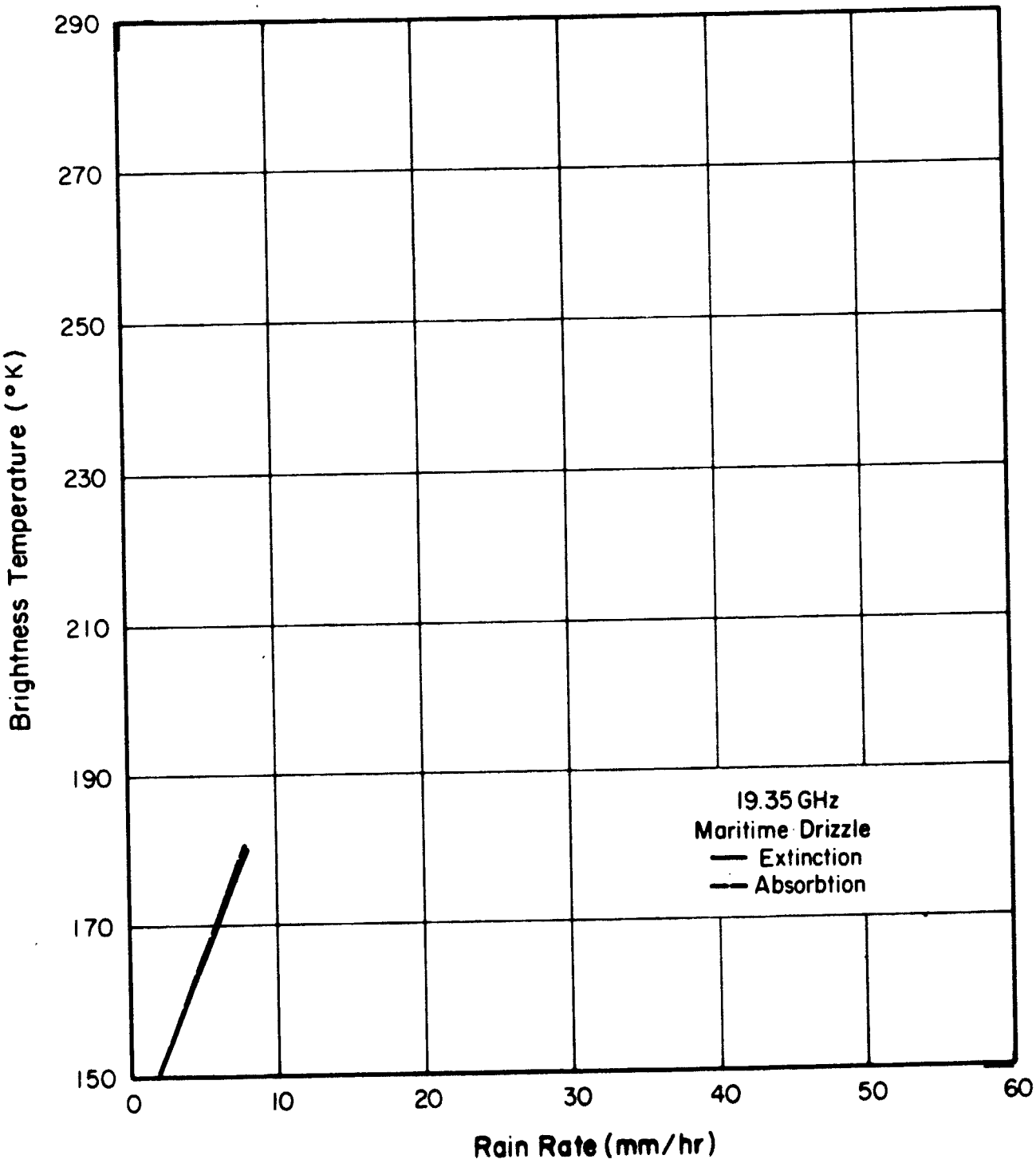

Figure 4-6 The Relationship Between Brightness Temperature and Rain Rate at 19.35 GHz for Maritime Drizzle.

in both cases. At very low rain rates there is little difference between the resulting brightness temperature, but this difference increases rapidly with increasing rain rate. Intuitively this is expected because at low rain rates the background, not the cloud, is the dominant source of emission and at high rain rates, the cloud top is the prime emitter.

More detailed analysis of the two cases, however, indicates that the differences are much smaller than would be expected. For example, the difference in the maximum extinction brightness temperatures between the two models is only 8° (268° versus 260°) while the cloud top temperatures differ by 27° (263° versus 236°). This indicates that the microwave sensor is "seeing" well into both clouds even at very high rain rates. The theory is supported by an examination of the layer contribution by the two clouds. The three-layer cloud shows a peak sensitivity to rain at the freezing level with contributions from all other levels. In contrast, the five layer cloud simply decreased in sensitivity with decreasing altitude but in such a fashion that the layer near the freezing level became the prime contributor to total emission. As a result, both clouds reached similar saturation microwave values.

Of even more importance, however, to the inference of rain rates, is the range of 2 to 20 mm/hr. In these cases, the total brightness temperatures for these rain rates differ by 10° or more leading to difficulties in predicting T_B's without a knowledge of the detailed cloud structure. Yet this does not prevent the inference of rain rates since the use of a selected brightness temperature generally causes an error of only 2 mm/hr in the estimated rain rate. In fact, the major difference between the two cases is in the critical rain rate beyond which the microwave sensor cannot discriminate values.

Figures 4-3 through 4-6 representing stratiform conditions in the midlatitudes show greater differences in the rain rate relationships, reflecting primarily the differences in atmospheric and surface temperature. The midlatitude summer case (Figure 4-3) bears a strong resemblance to the tropical cases discussed above because the temperature structure is quite similar and the integrated effects of the rain layers again produces the same microwave-rain rate relationship.

Of greater interest is the strong shift in the brightness temperatures when the spring/fall atmosphere is used (Figure 4-4). No longer

does the assumption of a certain brightness temperature/rain rate relationship lead to only a 2 mm/hr error. It can now cause a 10 mm/hr error. Since the drop size distributions and the cloud top temperature (273°) are identical for both the summer and fall cases, most of this difference must be due to the change in the temperature profile.

The values for the winter stratus case, also applicable to the arctic summer (Figure 4-5), show an even greater contrast to the midlatitude summer although they resemble the fall results. Again most of the change in the precipitation measurements appears due to the temperature of the atmosphere. This theory is supported by an examination of the maritime drizzle case shown in Figure 4-6. In this model, the distribution for drizzle is used with the midlatitude spring/fall atmospere and the differences between Figures 4-4 and 4-6 reflect only the effect of cloud microstructure. This effect is slight despite the fact that the drizzle drops are much smaller than the other raindrops simulated.

Figures 4-7 through 4-12 show the corresponding curves for the frequency of 37 GHz. These show a greater sensitivity to cloud structure (compare Figures 4-7 and 4-8) but still indicate that changes in the atmosphere are more significant than changes in cloud structure. In agreement with the findings for 19.35 GHz, changes in cloud structure have only small effects upon the inference of low rain rates. The most pronounced effect of changes in clouds is again upon the upper limit of rain rate which can be discriminated which varies from 40 mm/hr in Figure 4-7 to 15 mm/hr in Figure 4-8.

Comparison of the results for 19.35 GHz with those for 37 GHz supports that contention that the 19.35 GHz channel can clearly discriminate rain rates over a far greater range of values than can be inferred from 37 GHz. This is a direct consequence of the difference in the efficiency factor curves shown in Section 2 for the two frequencies. The findings are also encouraging in that the qualitative limits on sharp response to rain rate changes (15 mm hr^{-1} at 19.35 GHz and 7 mm hr^{-1} at 37 GHz) agree with the operational limits used for these frequencies (Wilheit, personal communication, 1975).

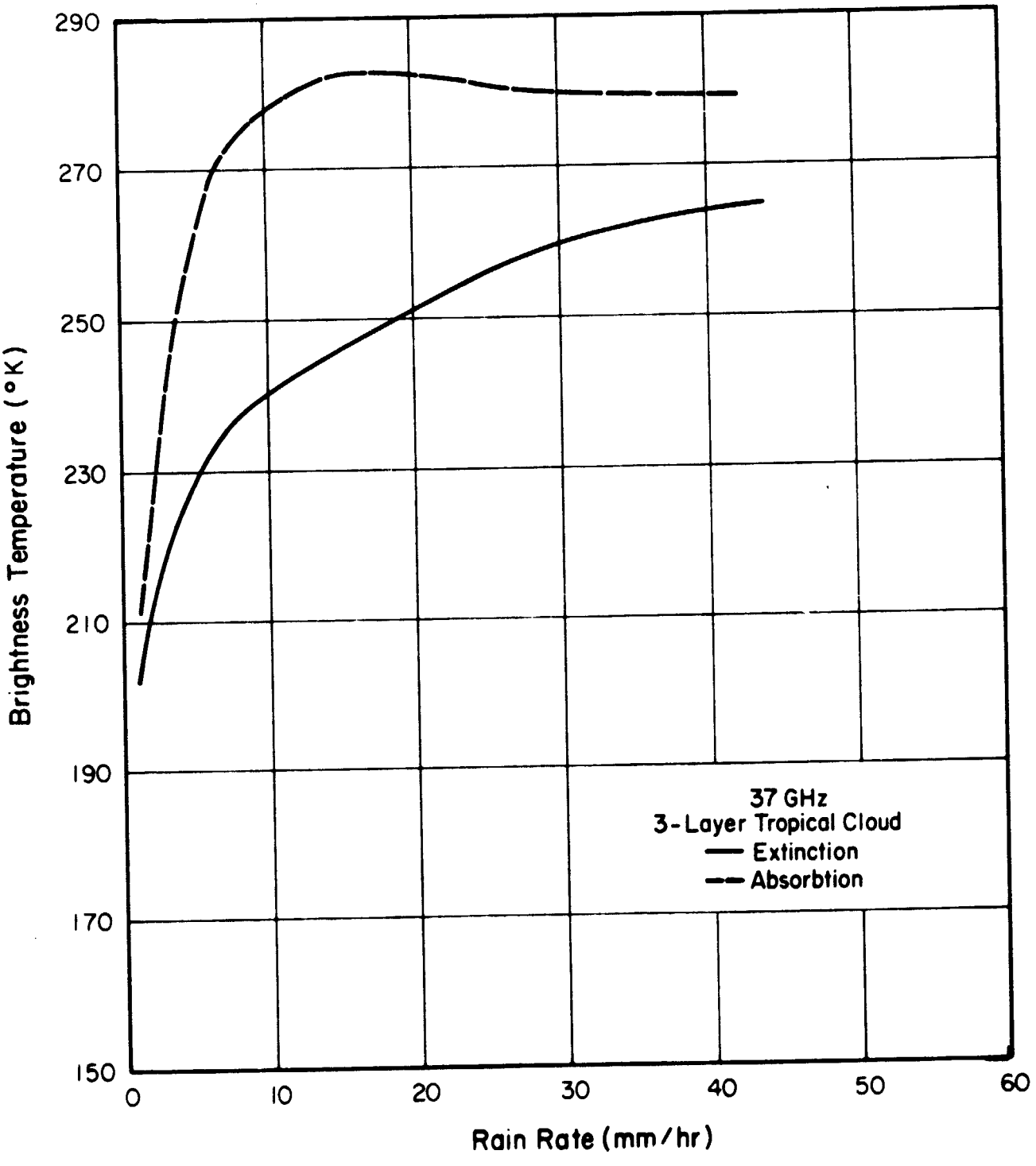

Figure 4-7 The Relationship Between Brightness Temperature and Rain Rate at 37.0 GHz for a Tropical Shower.

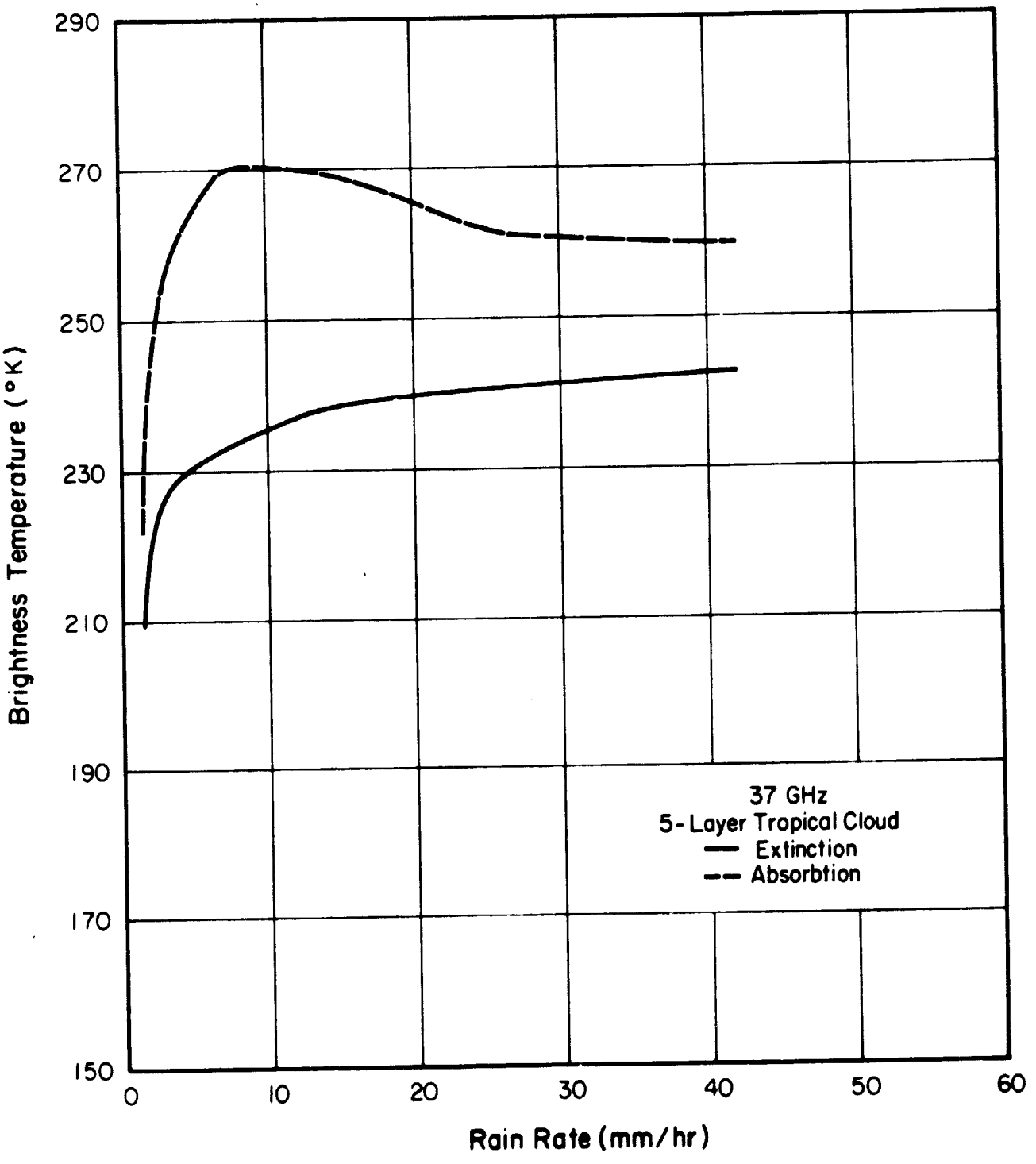

Figure 4-8 The Relationship Between Brightness Temperature and Rain Rate at 37.0 GHz for a Tropical Cumulonimbus.

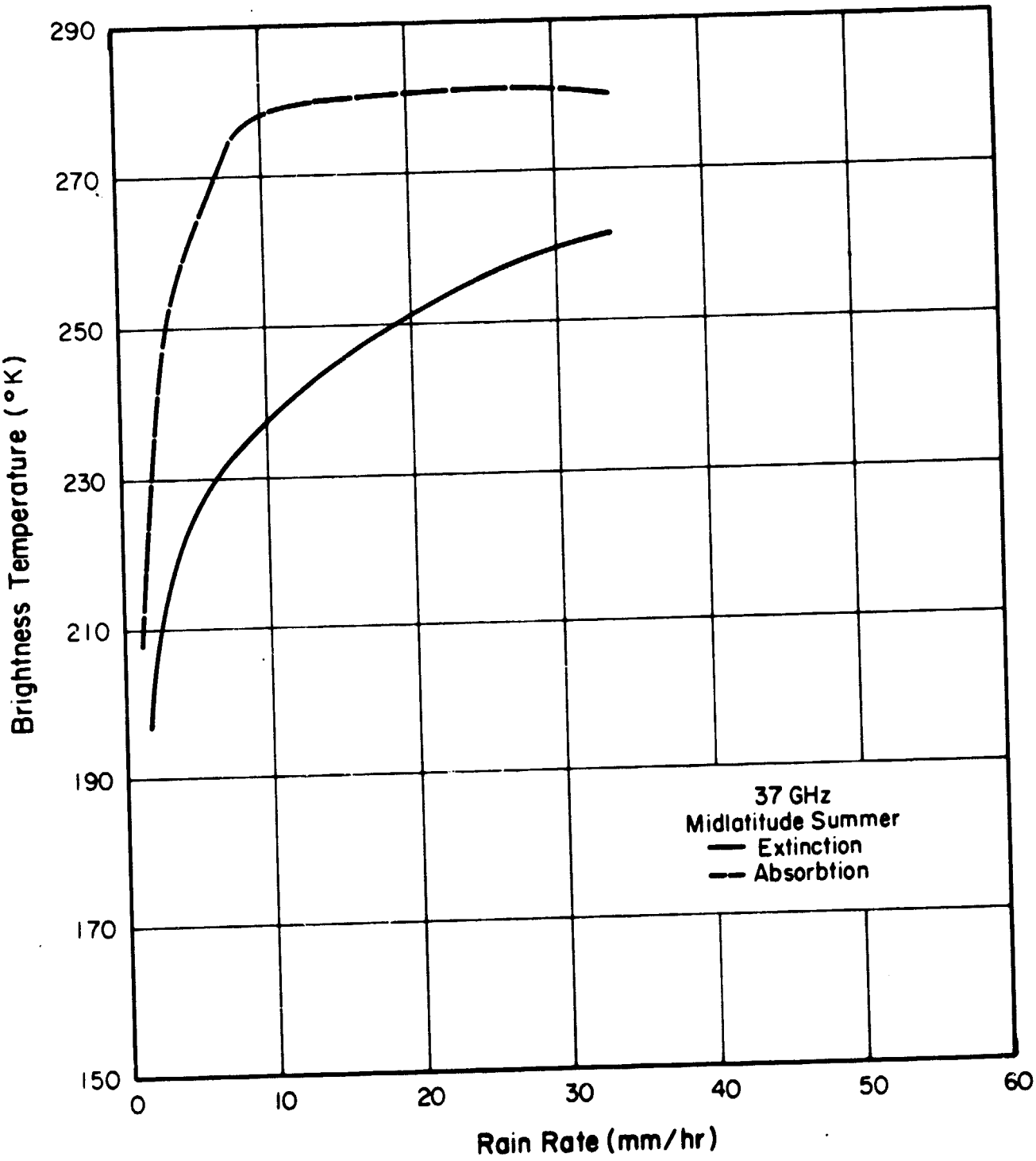

Figure 4-9 The Relationship Between Brightness Temperature and Rain Rate at 37.0 GHz for Midlatitude Summer Stratus.

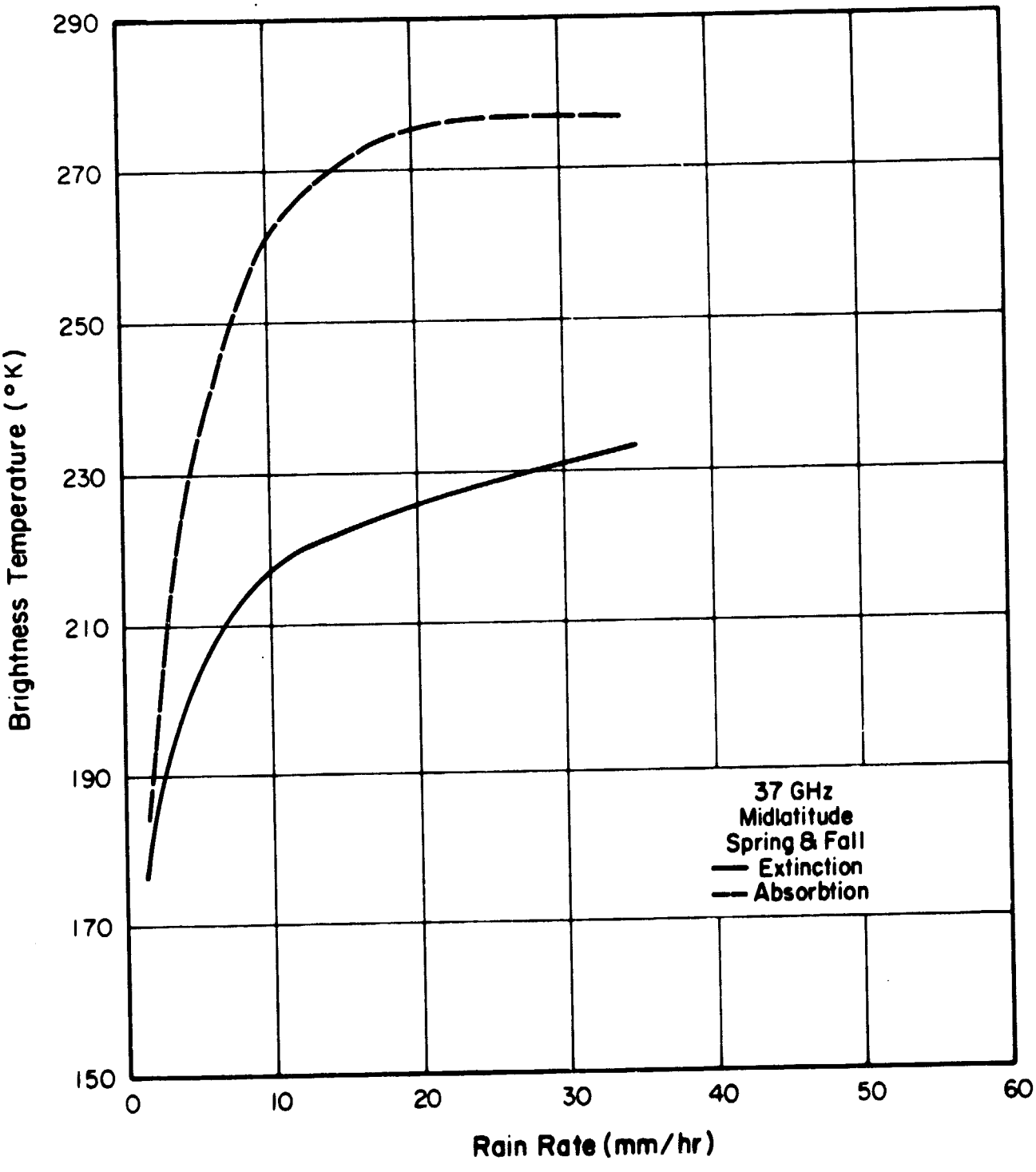

Figure 4-10 The Relationship Between Brightness Temperature and Rain Rate at 37.0 GHz for Midlatitude Spring/Fall Stratus.

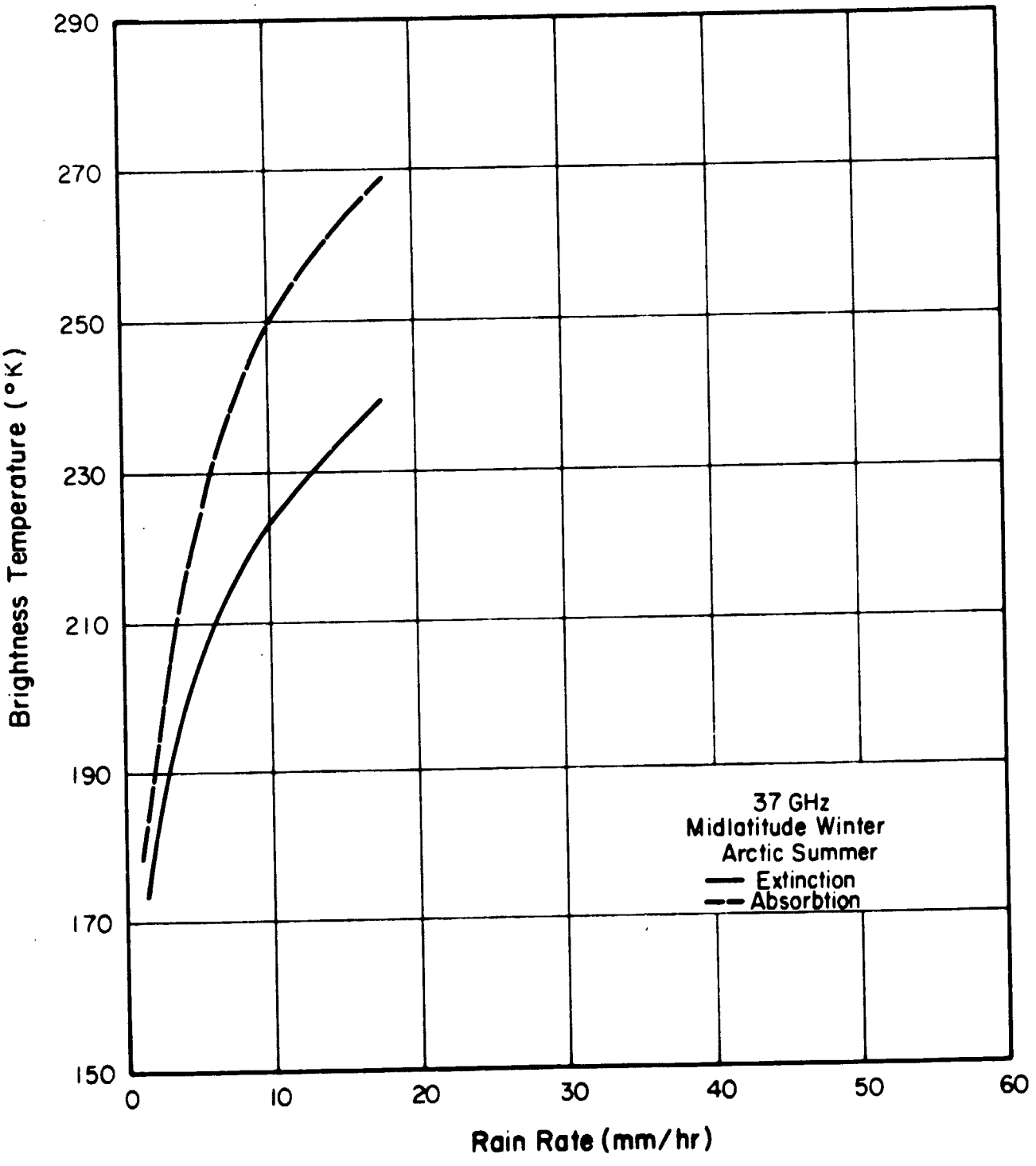

Figure 4-11 The Relationship Between Brightness Temperature and Rain Rate at 37.0 GHz for Midlatitude Winter Stratus.

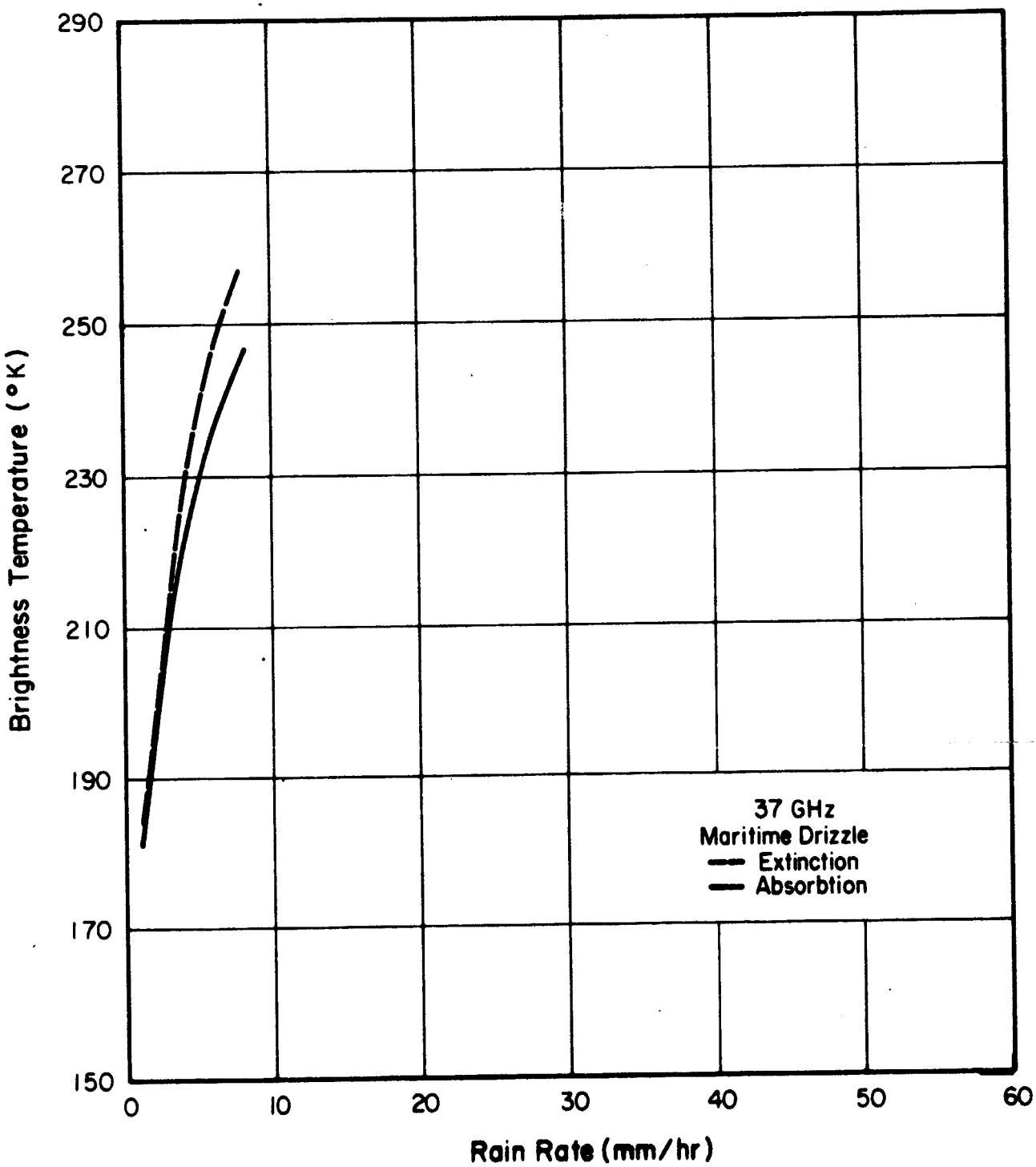

Figure 4-12 The Relationship Between Brightness Temperature and Rain Rate at 37.0 GHz for Maritime Drizzle.

4.2 Analysis of Microwave Sensitivity to Precipitation

To further investigate the finding that the relationship between microwave radiation and rain rate depends far more strongly upon the temperature of the raindrops than upon their size distribution, two additional sets of cases were run. Those shown in Figures 4-13 and 4-14 represent the same midlatitude spring/fall precipitation cases as was seen in Figures 4-4 and 4-10 except that the temperature profile was arbitrarily shifted up 5° and down 5°. The differences in the curves seen here for each frequency thus represents only differences in the temperatures of the rain layers. Little change is seen in the low rain rates where the background dominates but as the contribution due to raindrops increases, the brightness temperatures become increasingly dissimilar until they reach a difference of 6°. These differences cause only a small rain rate estimation error. However, since 10° changes in atmospheric temperature on a global basis are quite small, and since changes in the shape of the temperature profile and the surface temperature also occur, the variability of T_B is quite conservative and indicates the need of a statistical inversion approach to infer rain on a global basis.

The other set of cases examined fixed the atmosphere, cloud depth, and drop size distribution shape parameters, but varied the mode radius within the tropical shower cloud layers. Figures 4-15 and 4-16 show the resulting brightness temperatures for varying rain rates computed for 19.35 and 37 GHz. These domonstrate clearly that variations in drop size for meteorologically realistic conditions are not sufficient to cause marked changes in the microwave-rain rate relationship. However, the curves also show that, because of the shorter wavelength of the 37 GHz channel, that channel is much more sensitive to variations in drop size, although large errors in rain rate estimation still do not occur at low rain rates.

4.3 Summary

The relationship between microwave brightness temperature and rain rate is well-defined at both 19.35 and 37 GHz. This is a consequence of the strong dependence of both microwave emission and rain rate on larger

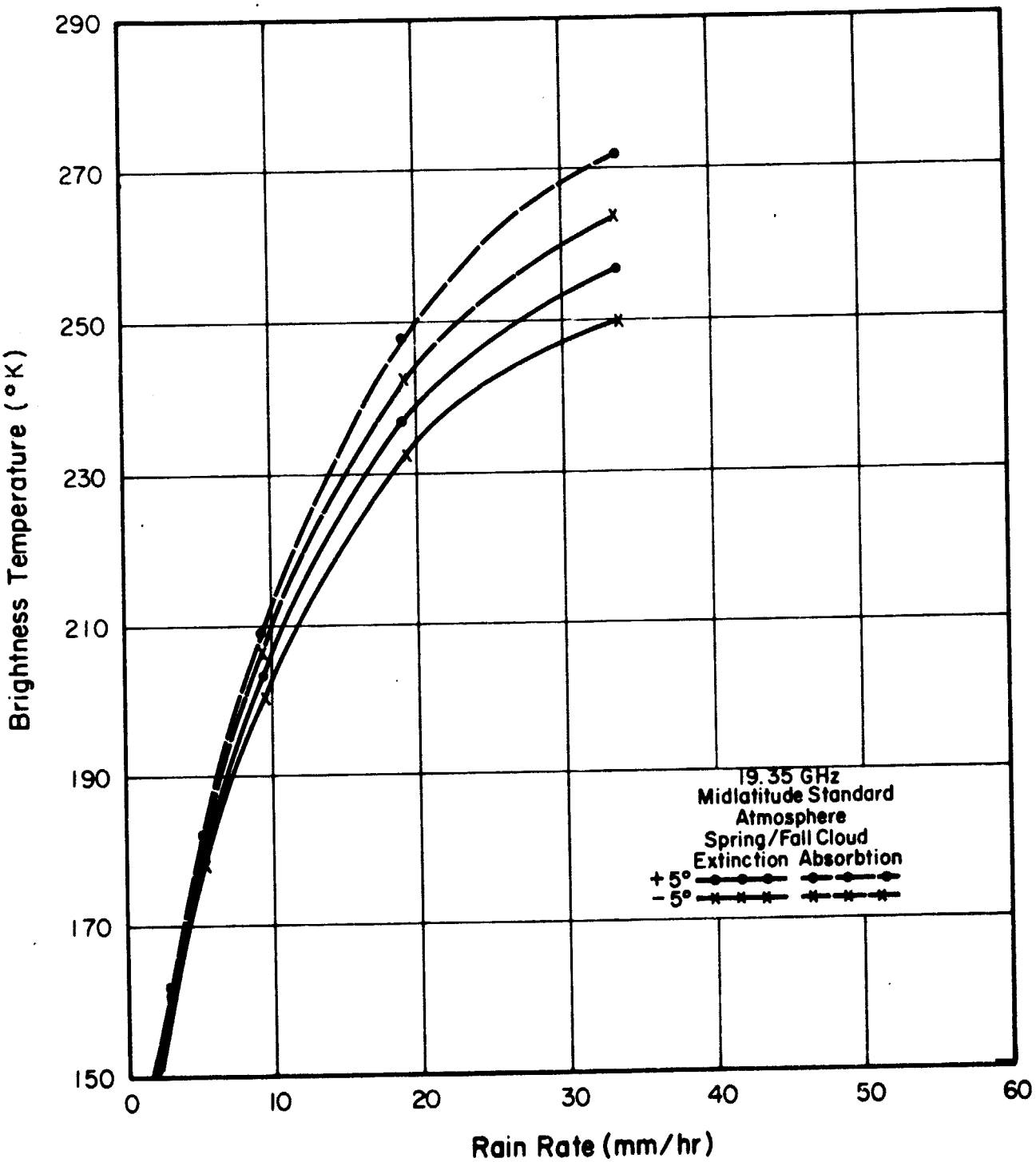

Figure 4-13 The Change in Brightness Temperature Due to a 5° Temperature Decrease in the Midlatitude Spring/Fall Atmosphere, 19.35 GHz.

604030
604087

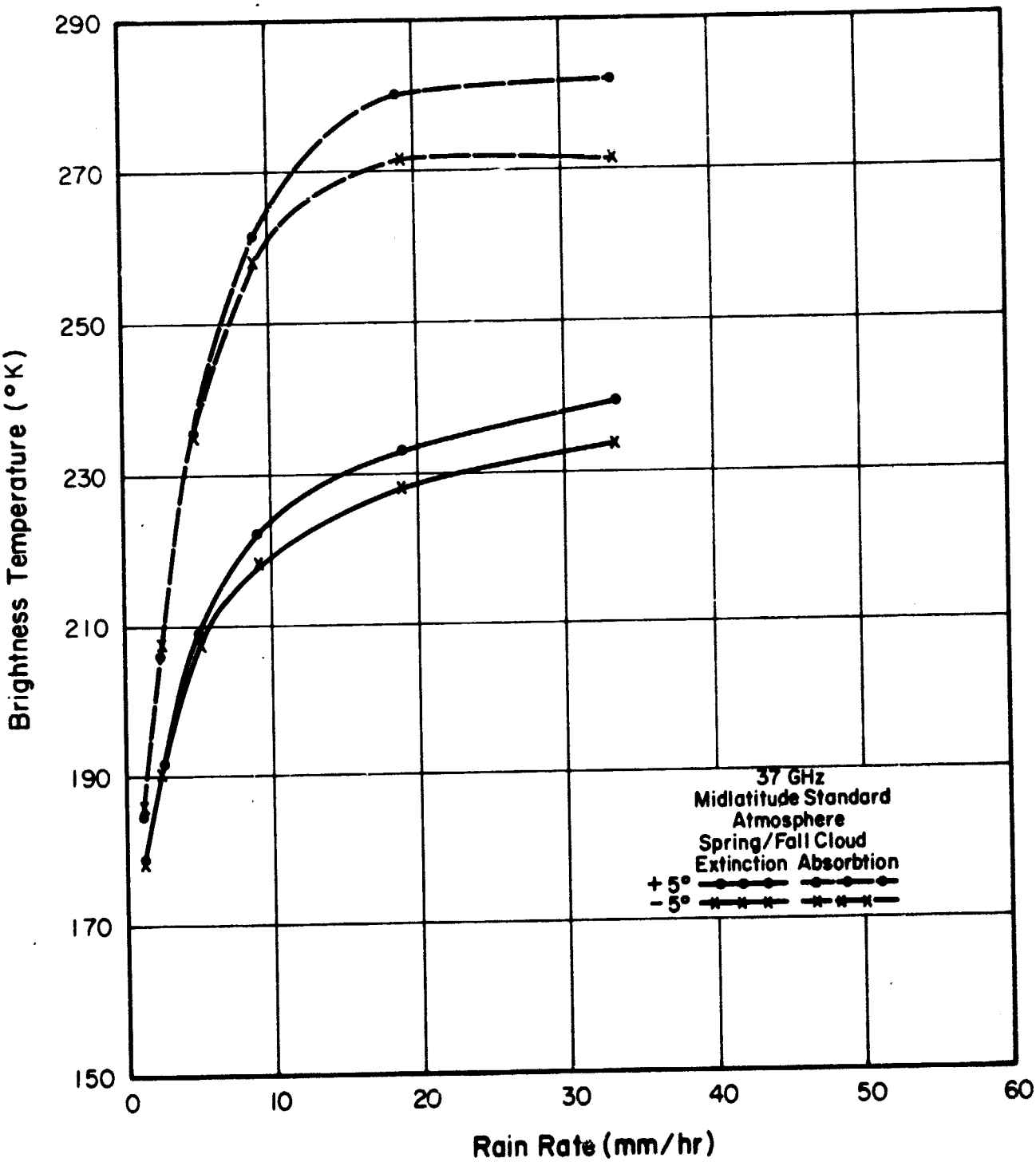

Figure 4-14 The Change in Brightness Temperature Due to a 5° Temperature Increase and a 5° Temperature Decrease in the Midlatitude Spring/Fall Atmosphere, 37.0 GHz.

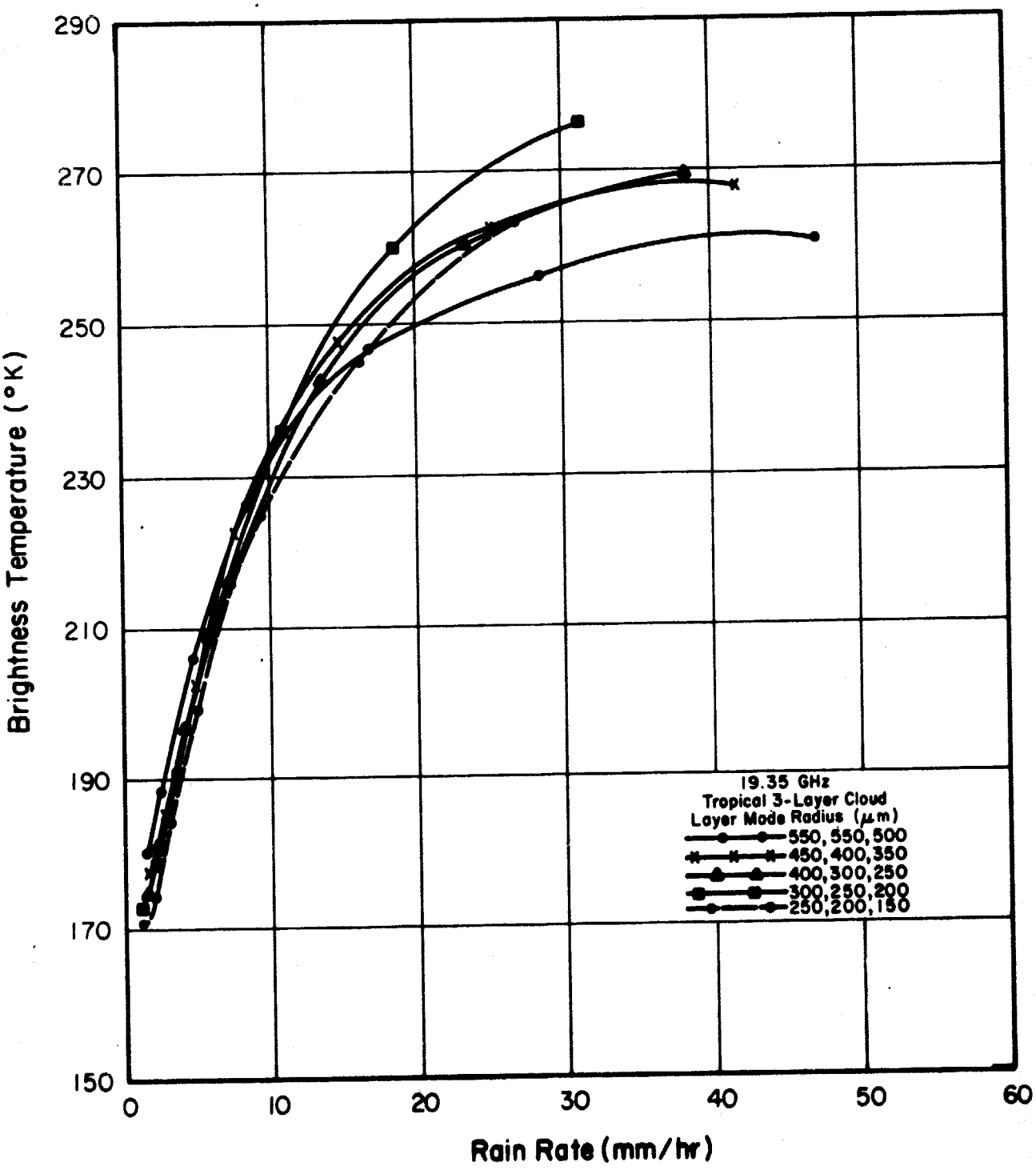

Figure 4-15 The Dependence upon the Mode Radius of the Brightness Temperature-Rain Rate Relationship, 19.35 GHz.

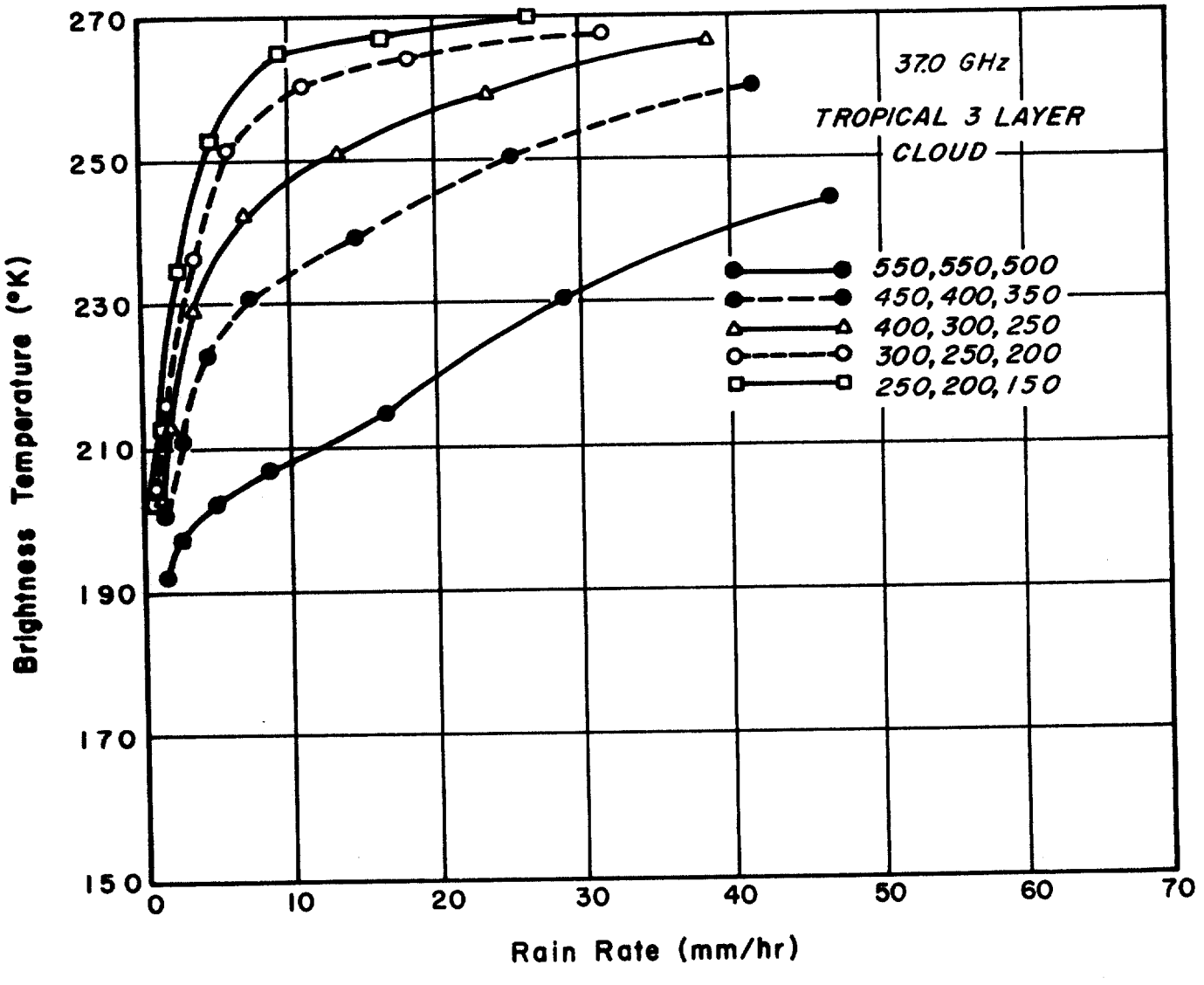

Figure 4-16 The Dependence upon the Mode Radius of the Brightness Temperature-Rain Rate Relationship, 37.0 GHz.

rain drops leading to a correlation between those parameters. Variability in this relationship becomes significant as the temperature of the rain layers varies, leading to wide ranges in T_B on a global and seasonal basis and requiring the use of a statistical inversion procedure to infer precipitation on an operational basis. However, the precipitation itself can be adequately modeled through the use of a few cloud models because the radiometric measurements are not highly sensitive to the drop size distribution.

5. CONCLUSIONS AND RECOMMENDATIONS

A radiometric model has been developed which approximates the effects of precipitation upon microwave radiation. This model does not utilize a full Mie scattering technique but rather permits the simulation and inversion of rain rates through the use of a computationally efficient technique. In terms of radiative interaction, this model assumes that the efficiency factors as a function of drop size can be approximated by four regimes: a Rayleigh regime, two transition regimes and a large sphere regime. Analytical expressions for these regions have been developed which can be used with either Marshall-Palmer or Deirmendjian distributions to determine the precipitation extinction coefficient. In addition, wavelength and temperature dependence have been incorporated into the model permitting its use in the numerical simulation of radiometric and atmospheric relationships. Comparison of the extinction coefficients and microwave brightness temperatures with those computed from full Mie theory show that this model provides reliable results.

In conjunction with the radiometric model, precipitating cloud models have been developed which describe the vertical structure of raindrop spectra for differing cloud types and climatic conditions in terms of Deirmendjian distributions. These models, with their appropriate atmospheres, have been simulated through the use of ERT's radiometric model to determine the relationship between brightness temperature and rain rates for frequencies of 19.35 and 37.0 GHz. The results of this simulation showed that this relationship is highly dependent upon the temperature structure of the atmosphere. Less sensitivity to the cloud microstructure was found because rain rate and microwave extinction are both highly dependent upon the density of large drops.

It is recommended that a statistical inversion procedure be used to infer precipitation from radiometric measurements because of the high variability in brightness temperature due to changes in atmospheric temperature structure. Through the use of this procedure, accurate estimates of rain rate can be made on a global basis from measurements made at the frequencies discussed above.

6. REFERENCES

Battan, Louis J., 1973: Radar Observation of the Atmosphere, University of Chicago Press, 324 p.

Chandrasekar, S., 1960: Radiative Transfer, Dover Press, New York.

Chang, D.T. and J.H. Willand, 1972: Further Developments in Cloud Statistics for Computer Simulations, NASA CR-61389.

Crane, R.K., 1972: Virginia Precipitation Scatter Experiment - Data Analysis, NASA/GSFC X-750-73-55, NASA Goddard Space Flight Center.

Debye, P., 1929: Polar Molecules, Dover Press.

Deirmendjian, D., 1964: "Scattering and Polarization Properties of Water Clouds and Hazes in the Visible and Infrared", Applied Optics, 3(2), p. 187.

Fowler, M.G., N.D. Sze and N.E. Gaut, 1975: The Estimation of Clear Sky Emission Values from Cloudy Radiometric Data, AFCRL-TR-75-0440, Final Report Contract No. F19628-75-C-0035, Environmental Research & Technology, Inc.

Gaut, N.E., M.G. Fowler, R.G. Isaacs, D.T. Chang and E.C. Reifenstein, III, 1974: Studies of Microwave Remote Sensing of Atmospheric Parameters, AFCRL-TR-75-0007, Final Report Contract No. F19628-73-C-0195, Environmental Research & Technology, Inc.

Gaut, N.E. and E.C. Reifenstein, III, 1970: Interaction of Microwave Energy Within the Atmosphere, paper presented at AIAA Earth Resources Observations and Information Systems, Annapolis, Md., ERT Technical Report No. 10.

Gaut, N.E. and E.C. Reifenstein, III, 1971: Interaction Model of Microwave Energy and Atmospheric Variables, Final Report Contract No. NAS 8-26275, (NASA CR-61348), Environmental Research & Technology, Inc.

Gaut, N.E., E.C. Reifenstein, III and D.T. Chang, 1972: Microwave Properties of the Atmosphere, Clouds and the Oceans, Final Report Contract No. NAS5-21194, Environmental Research & Technology, Inc.

Grant, E.H., T.J. Buchanan and H.F. Cook, 1957: "Dielectric Behavior of Water and Microwave Frequencies", J. Chem. Phys., Vol. 26.

Gunn, R. and G.D. Kinzer, 1949: "The Terminal Velocity of Fall for Water Droplets in Stagnant Air", J. Met., Vol. 6.

Hardy, K.R., 1963: "The Development of Raindrop-Size Distributions and Implications Related to the Physics of Precipitation", J. of Atmos. Sci., Vol. 20, No. 4.

Joss, J., R. Cavalli and R.K. Crane, 1974: "Good Agreement Between Theory and Experiment for Attenuation Data", J. de Recherches Atmospheriques, Vol. 8, p. 299-318.

Marshall, J.S. and W.M. Palmer, 1948: "The Distribution of Raindrops with Size", J. Meteor., Vol. 5.

Mason, B.J. and R. Ramanadham, 1954: "Modification of the Size Distribution of Falling Raindrops by Coalescence", Q. Jour. Royal Met. Soc., Vol. 80.

Mie, G., 1908: Ann. Phys., Vol. 24.

Ohtake, T., 1969: "Observation of Size Distribution of Hydrometers Through the Melting Layer", Proc. of the Thirteenth Radar Meteor. Conf., Boston Amer. Meteor. Soc.

Reifenstein, E.C., III and N.E. Gaut, 1971: Microwave Properties of Clouds in the Spectral Range 30-40 GHz, Final Report, ERT Project No. P-060 for NASA Goddard Space Flight Center, Contract NAS5-21194.

Rigby, E.C., J.S. Marshall and W. Hitschfield, 1954: "The Development of the Size Distribution of Raindrops During their Fall", J. Met., Vol. 2.

Shifrin, K.S. and M.M. Chernyak, 1970: "Absorption and Scattering of Microwaves in Precipitation", in Transfer of Microwave Radiation in the Atmosphere, K.S. Shifrin (ed), Israeli Program for Scientific Translations.

Staelin, D.H., 1966: "Measurements and Interpretations of the Microwave Spectrum of the Terrestrial Atmosphere Near 1-Centimeter Wavelength", J. Geophys. Res., 7(1).

Westwater, E.R. and O.N. Strand, 1965: Application of Statistical Estimation Techniques to Ground-Based Passive Probing of the Tropospheric Structure, ESSA Technical Report No. IER 371/1TSA 37.

Wilheit, T.T. and M.G. Fowler, 1976: "Microwave Radiometric Determination of Wind Speed at the Surface of the Ocean During Besex", to be published in IEEE, AP Special Issue of Radio Oceanography.

Wilheit, T.T., M.S.V. Rao, T.C. Chang, E.B. Rodgers and J.S. Theon, 1975: A Satellite Technique for Quantitatively Mapping Rainfall Rates Over the Oceans, X-911-75-72, NASA Goddard Space Flight Center.

Willand, J.H., M.G. Fowler, E.C. Reifenstein, III and D.T. Chang, 1973: Analysis of Aircraft Microwave Measurements of the Ocean Surface, Final Report, NAS 5-21828, Environmental Research & Technology, Inc.

Young, K.C., 1975: "The Evolution of Drop Spectra through Condensation, Coalescence and Breakup", J. Atmos. Sci., 32.